



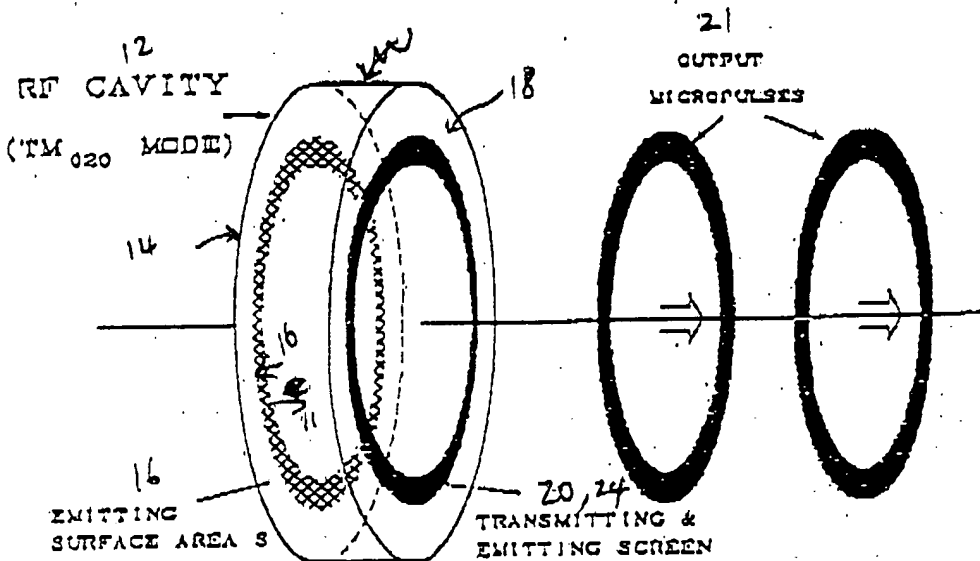
22
oscillating means
28
magnetic field means

10 electron gun

RECEIVED

JUL 01 2004

TECH CENTER 2800



11 : electrons between 16 and 20

Figure 1: Perspective view of the micropulse gun for a hollow beam in the TM_{020} mode. The inner conductor is not shown.

SUBSTITUTE FIGURE



TM-020 Mode Cavity with Inner Cylinder

10 electron gun

RECEIVED

JUL 01 2004

TECH CENTER 2800

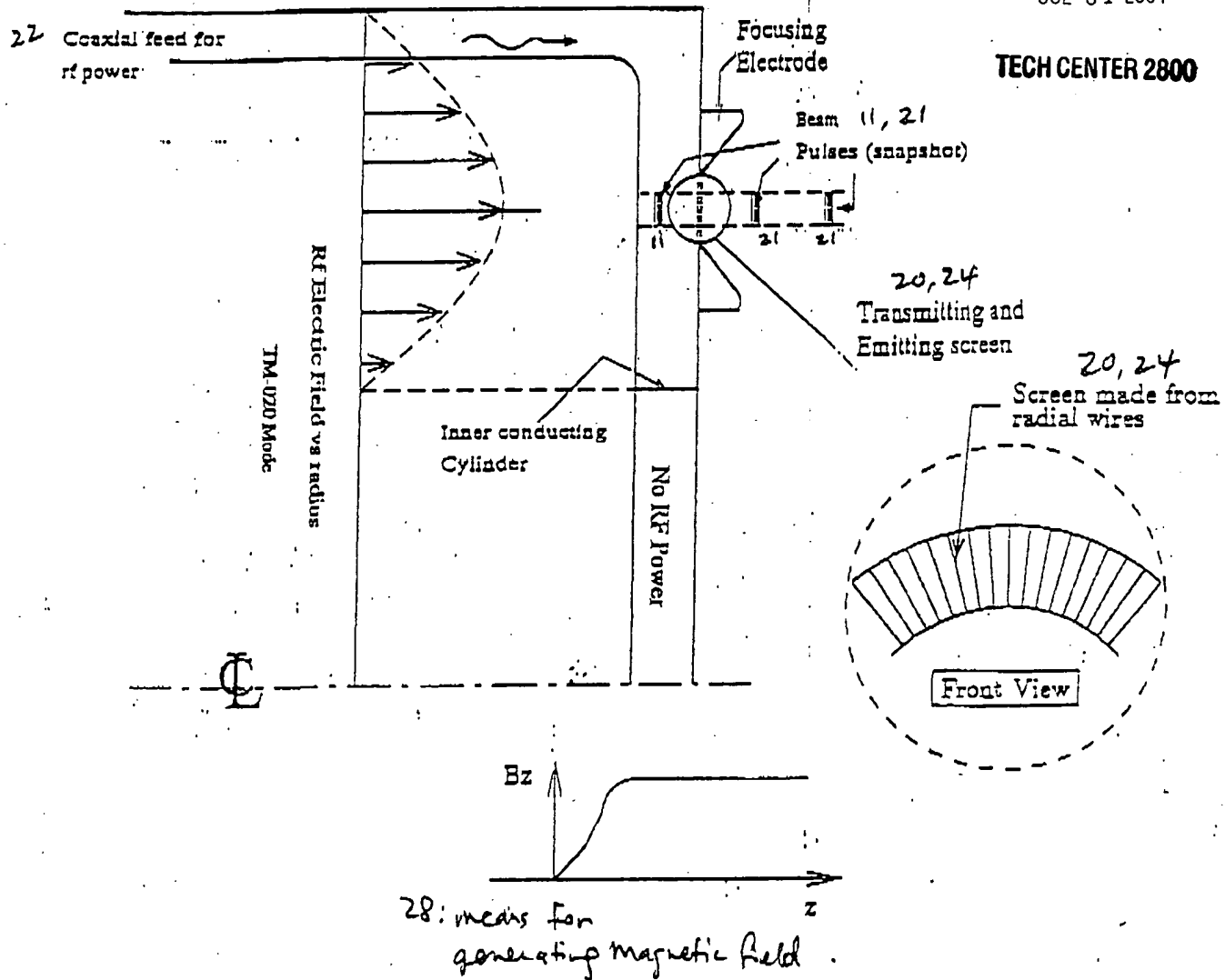


Figure 2: Schematic of rf gun operating in TM₀₂₀ mode.

SUBSTITUTE FIGURE



OSCILLATING
MEANS
22
OSCILLATING E
FIELD 26

Focusing
~~OSCILLATING~~
B. FIELD 28
MEANS

RF cavity
(side view)

10

RECEIVED

JUL 01 2004

TECH CENTER 2800

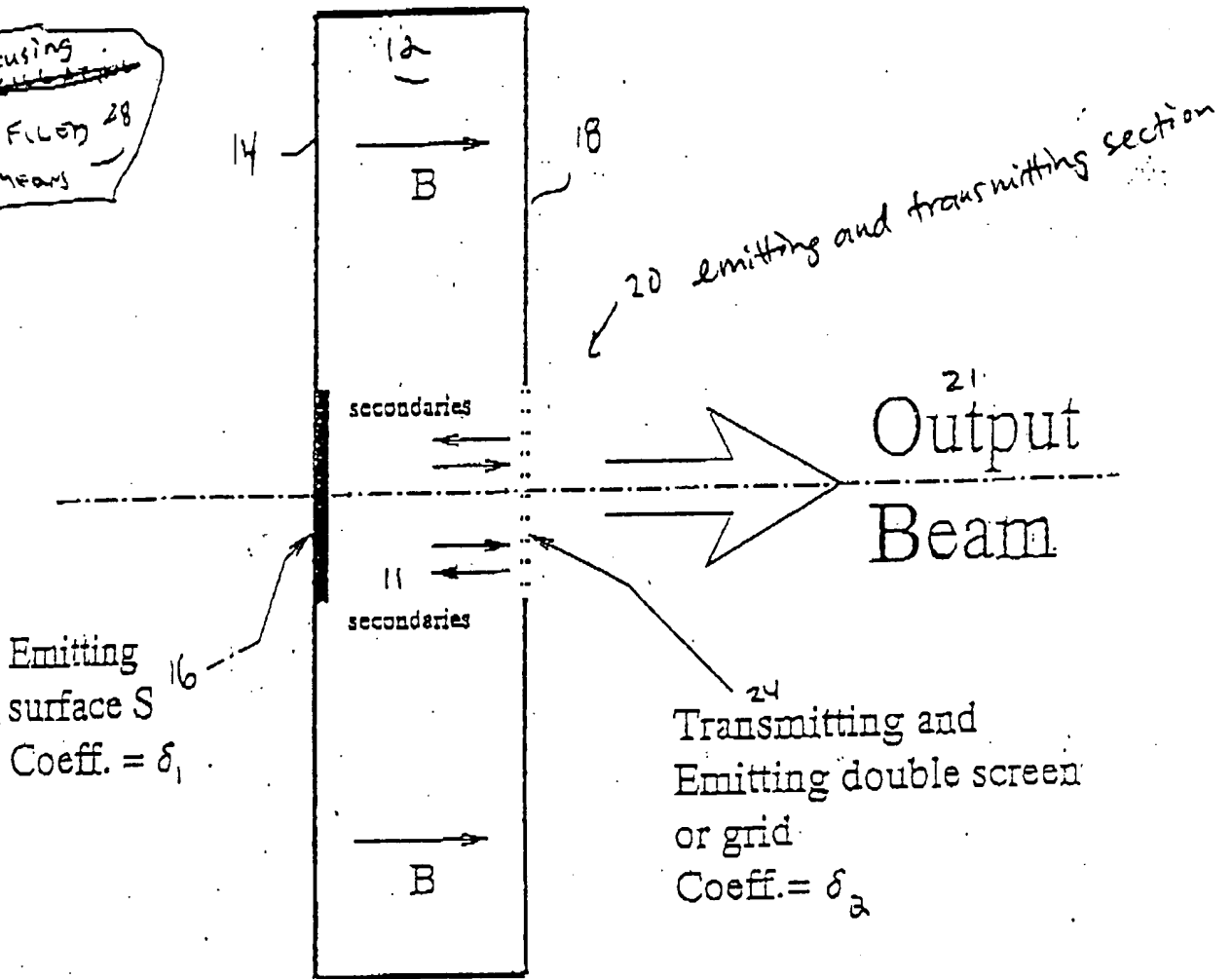


Figure 3: Schematic of micropulse gun for solid beam (TM_{010}) mode. A coaxial feed is used for rf input (not shown).

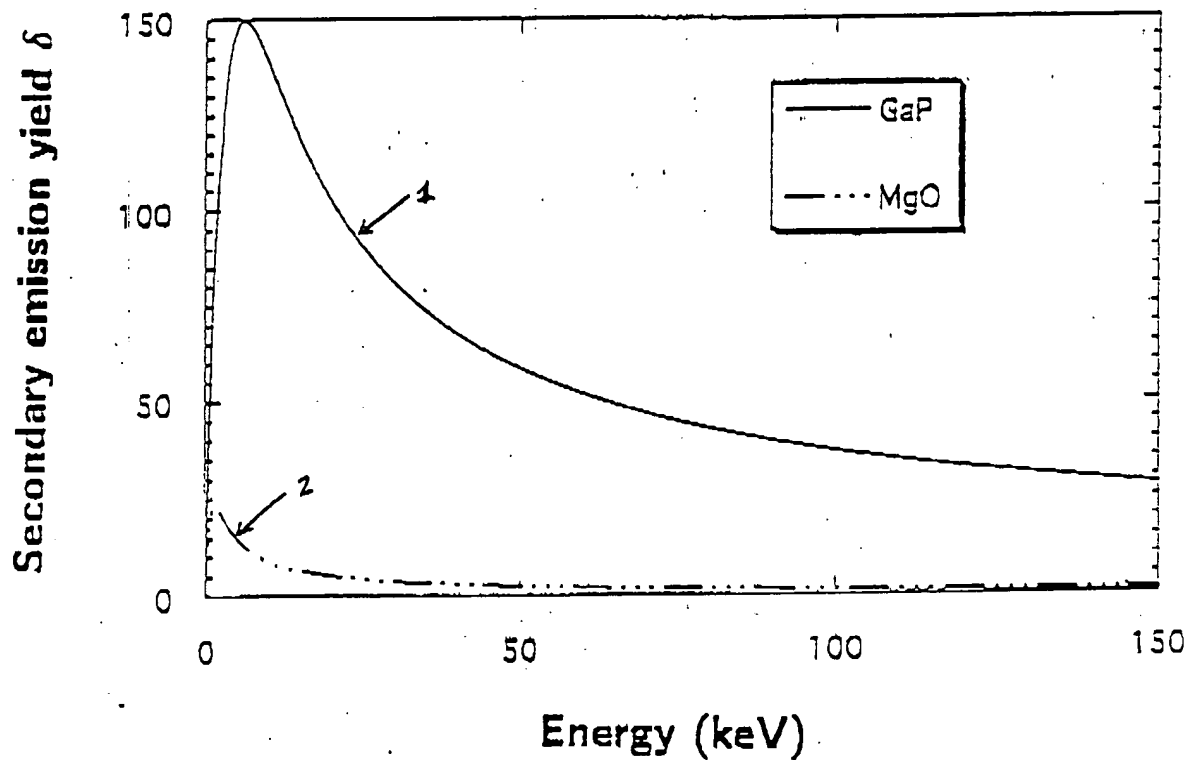
SUBSTITUTE FIGURE



RECEIVED

JUL 01 2004

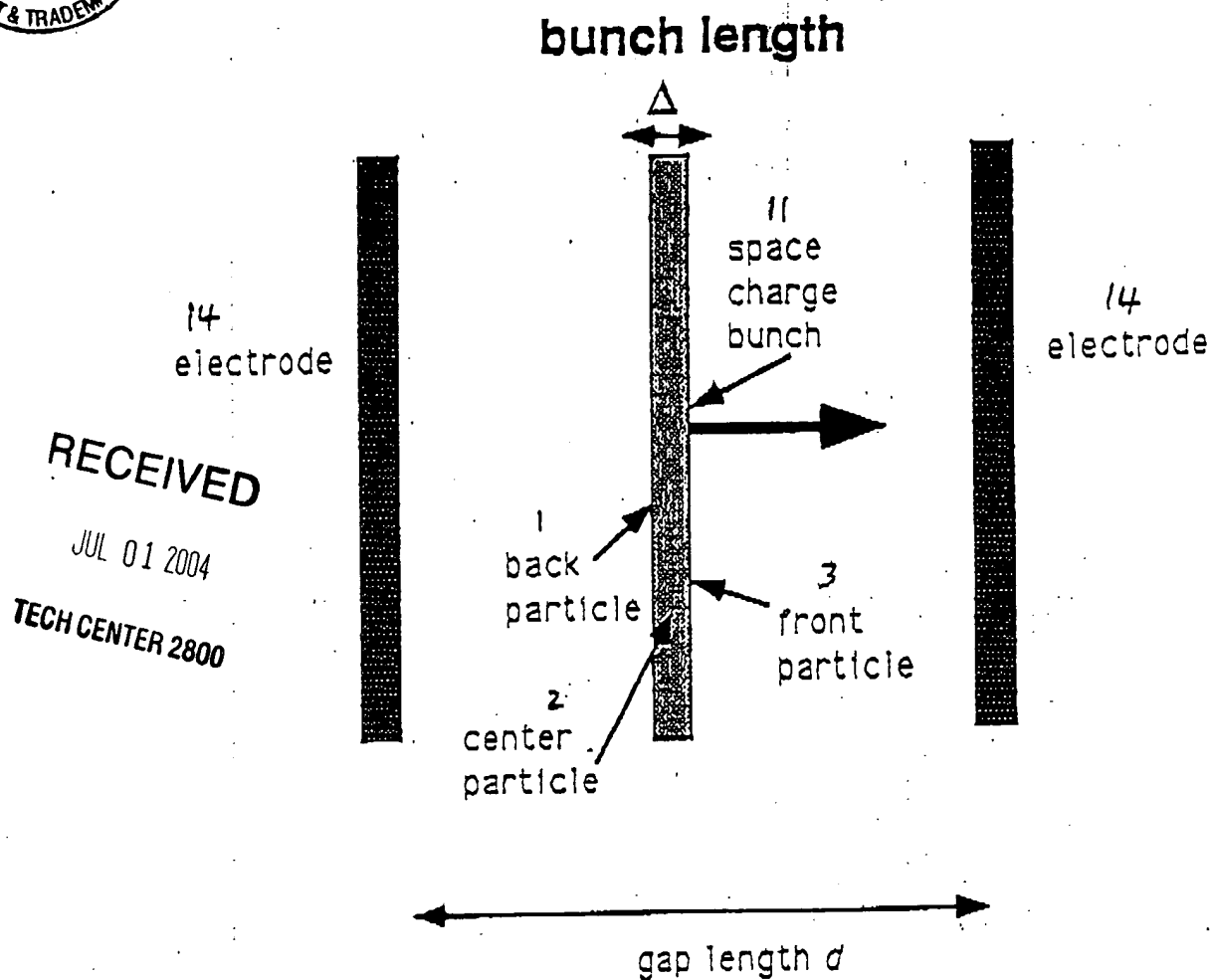
TECH CENTER 2800



1: Secondary emission yield of GaP
2: " " " " " " MgO

Figure 4: Secondary electron emission yield curve for GaP and MgO

SUBSTITUTE FIGURE



- 14 : emitting electrodes
- 11 : Electron bunch
- 1 : A back particle/electron
- 2 : " center " "
- 3 : " front " "

Figure 5: Schematic drawing of model used in theoretical analysis.

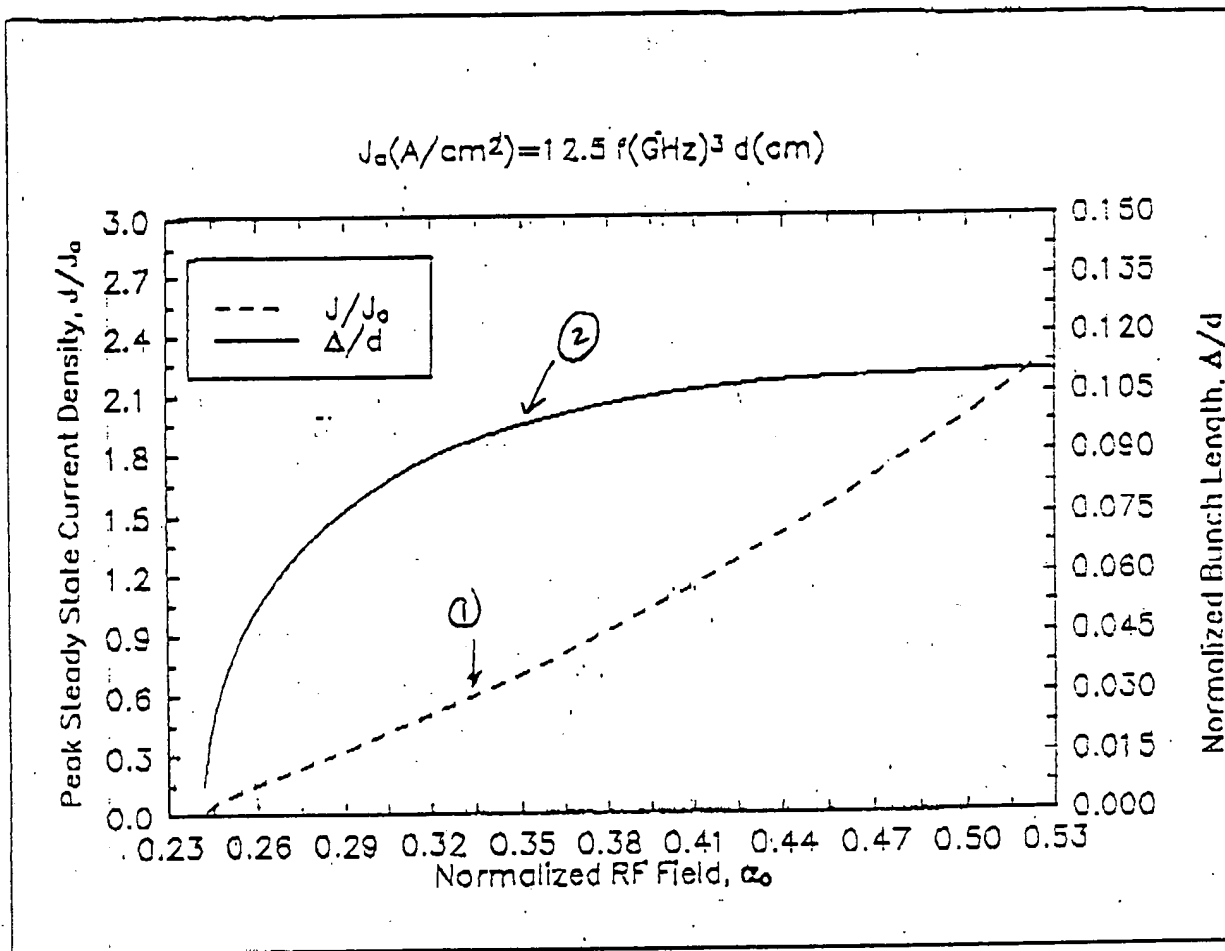
SUBSTITUTE FIGURE



RECEIVED

JUL 01 2004

TECH CENTER 2800



- ① Plot of ^{normalized} Peak current density at steady state versus RF field
- ② " ^{normalized} electron bunch length versus RF field.

Figure 6: Steady-state current density and bunch length vs. rf field, all parameters are normalized.

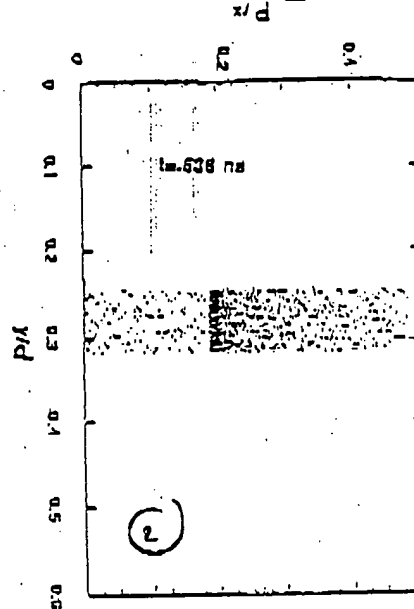
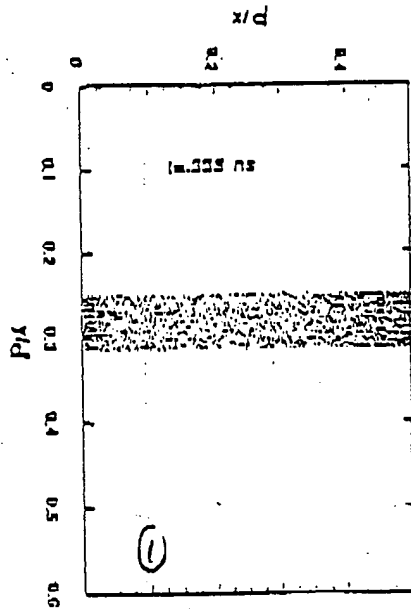
SUBSTITUTE FIGURE

TECH CENTER 2800



1.3 GHz, xy plot

- ① Plot of electron distribution in the cavity at $t = 0.335 \text{ ns}$.
- ② at $t = 0.636 \text{ ns}$
- ③ at $t = 2.462 \text{ ns}$
- ④ at $t = 3.35 \text{ ns}$



RECEIVED

JUL 01 2004

TECH CENTER 2800

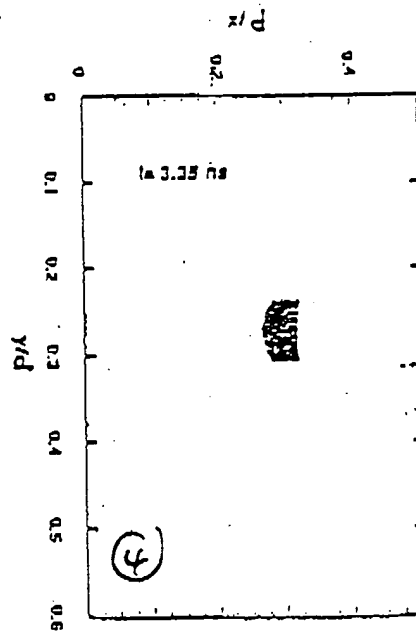
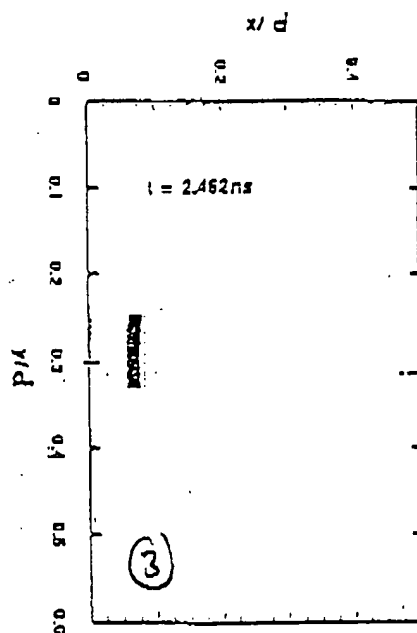


Figure 8: Series of time "snapshots" for a 1.3 GHz, $d = 0.5 \text{ cm}$ cavity using the two-dimensional PIC code with secondary emission. Note the rapid particle build-up and bunching by phase selection. Electrons traverse the horizontal axis. On the vertical axis emission is limited to the region 0.25 to 0.32 cm.

SUBSTITUTE FIGURE



RECEIVED

JUL 01 2004

TECH CENTER 2800

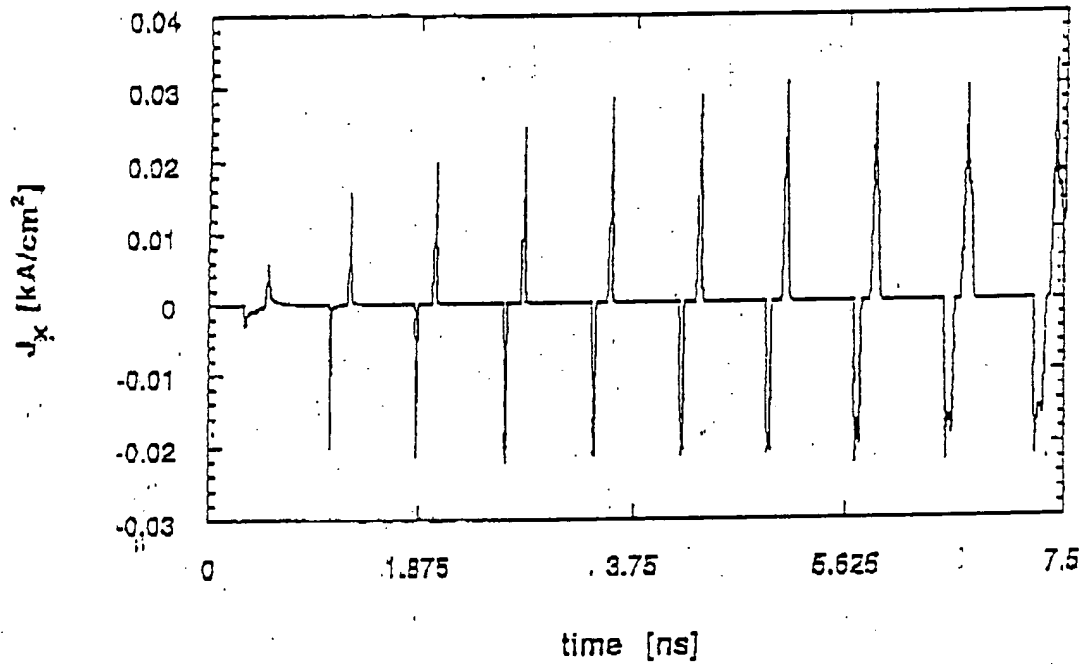


Figure 9: Plot of current density vs. time for simulation with rf frequency 1.3 GHz, voltage amplitude 4.3 kV, $d = 0.5$ cm, and $\alpha_0 = 0.453$.



RECEIVED

JUL 01 2004

TECH CENTER 2800

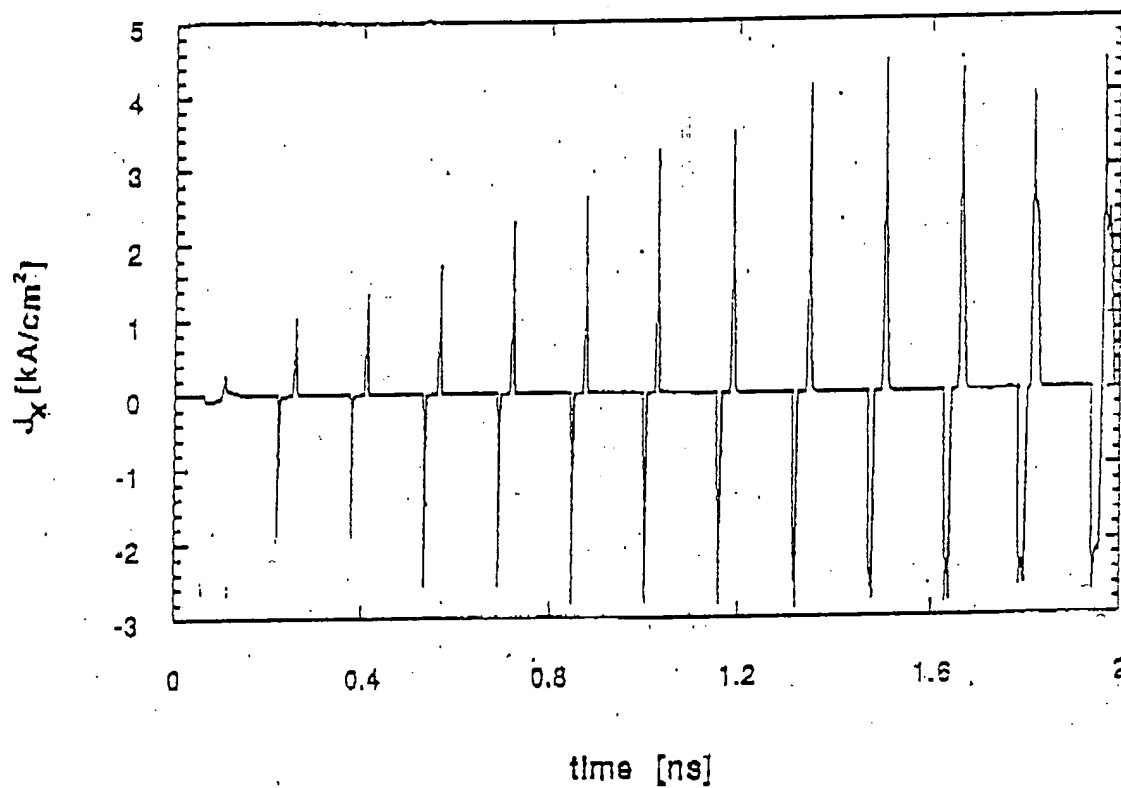


Figure 10: Plot of current density vs. time for simulation with rf frequency 6.4 GHz, voltage amplitude 105 kV, $d = 0.5$ cm, and $\alpha_0 = 0.453$.



RECEIVED

JUL 01 2004

TECH CENTER 2800

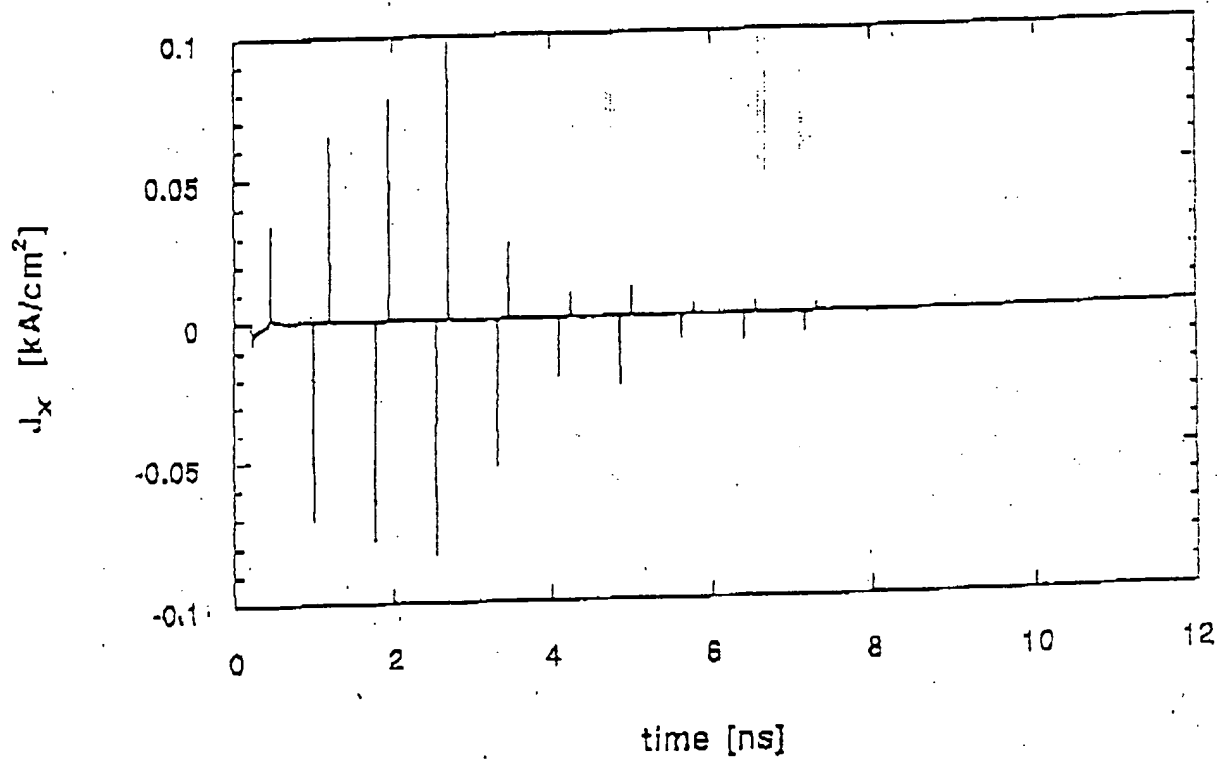


Figure 11: Current density in kA/cm^2 for an off-resonance $d = 0.5$ cm cavity with frequency 1.3 GHz and higher voltage 9.8 kV. Note that not only does current amplification not occur, but the steady-state current is zero.



RECEIVED

JUL 01 2004

TECH CENTER 2800

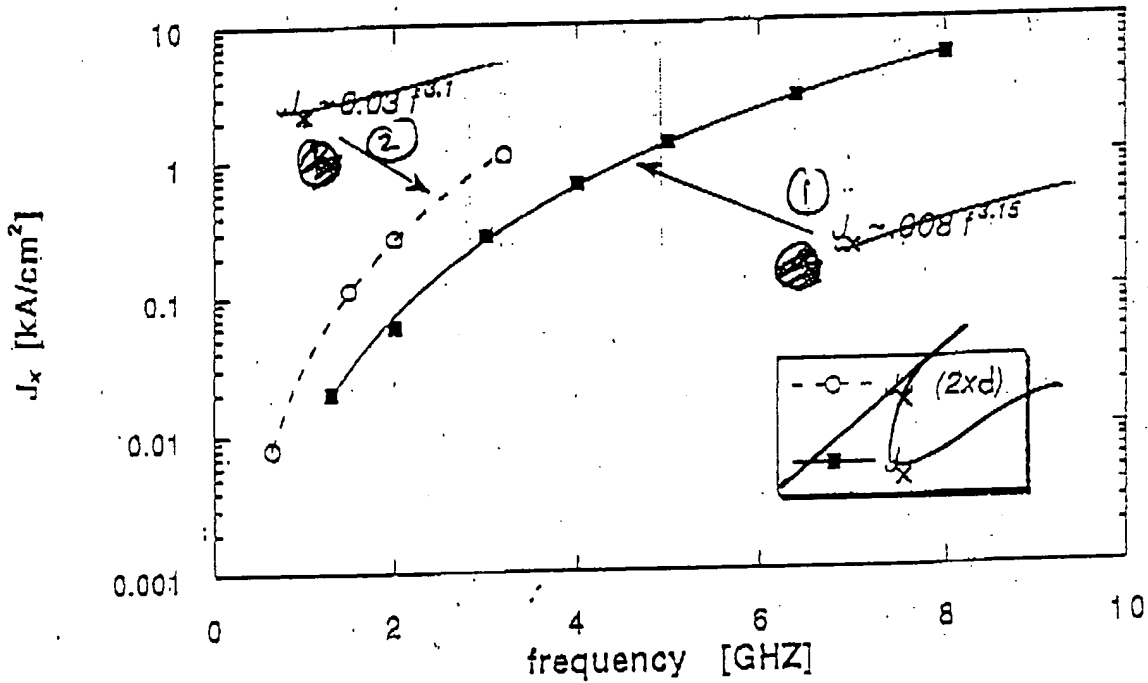


Figure 12: Steady-state current density vs. rf frequency for cavity with $\alpha_0 = 0.453$ and gap lengths of (1) 0.5 cm (solid line) and (2) 1.0 cm (dashed line)

is a fit using $J_x = 0.008 f^{3.15}$

is a fit using $J_x = 0.03 f^{3.1}$

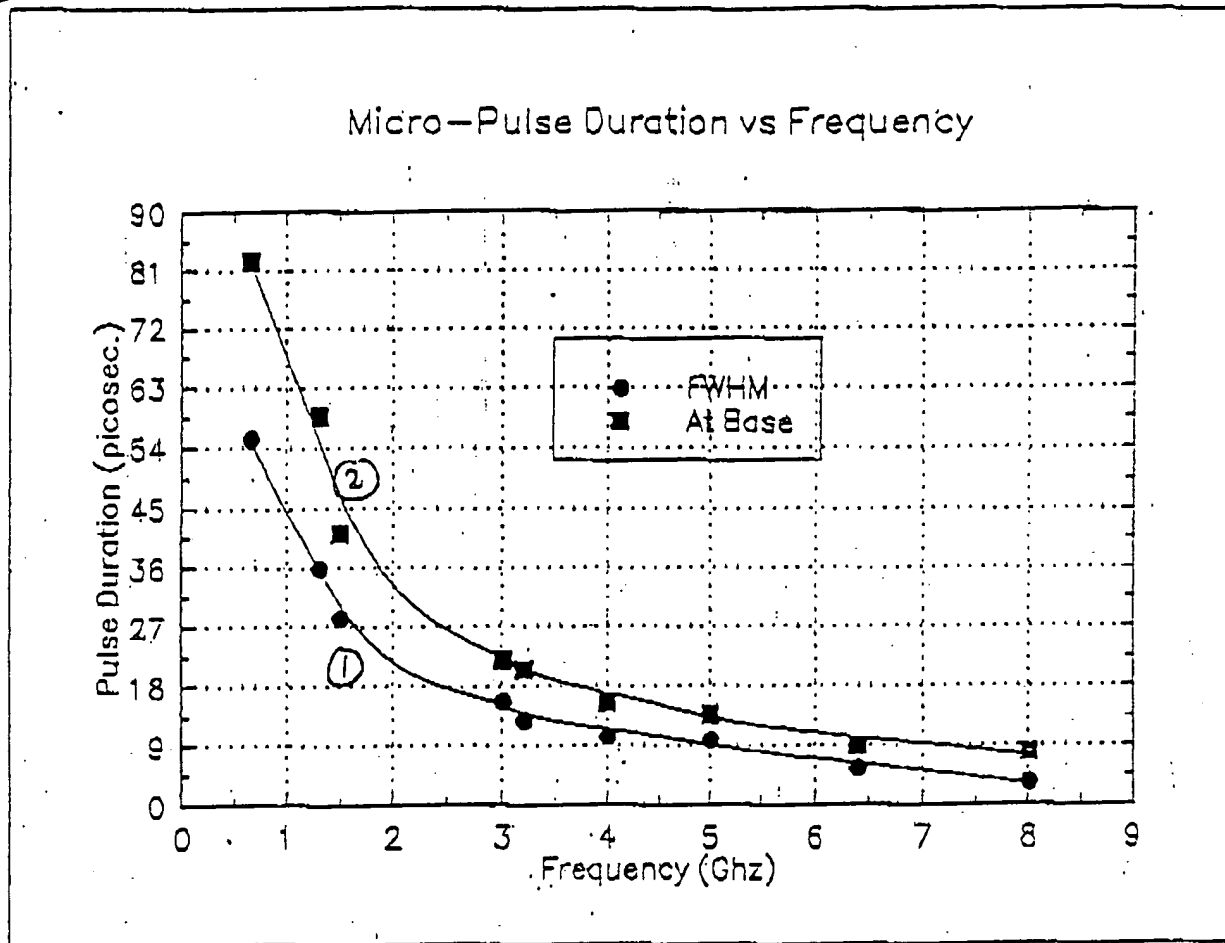
SUBSTITUTE FIGURE



RECEIVED

JUL 01 2004

TECH CENTER 2800



- ① Electron micro-pulse full width at half maximum.
② " " " " " " the base of the pulse.

Figure 13: Micro-pulse duration vs. frequency for $\alpha_0 = 0.453$.

SUBSTITUTE FIGURE

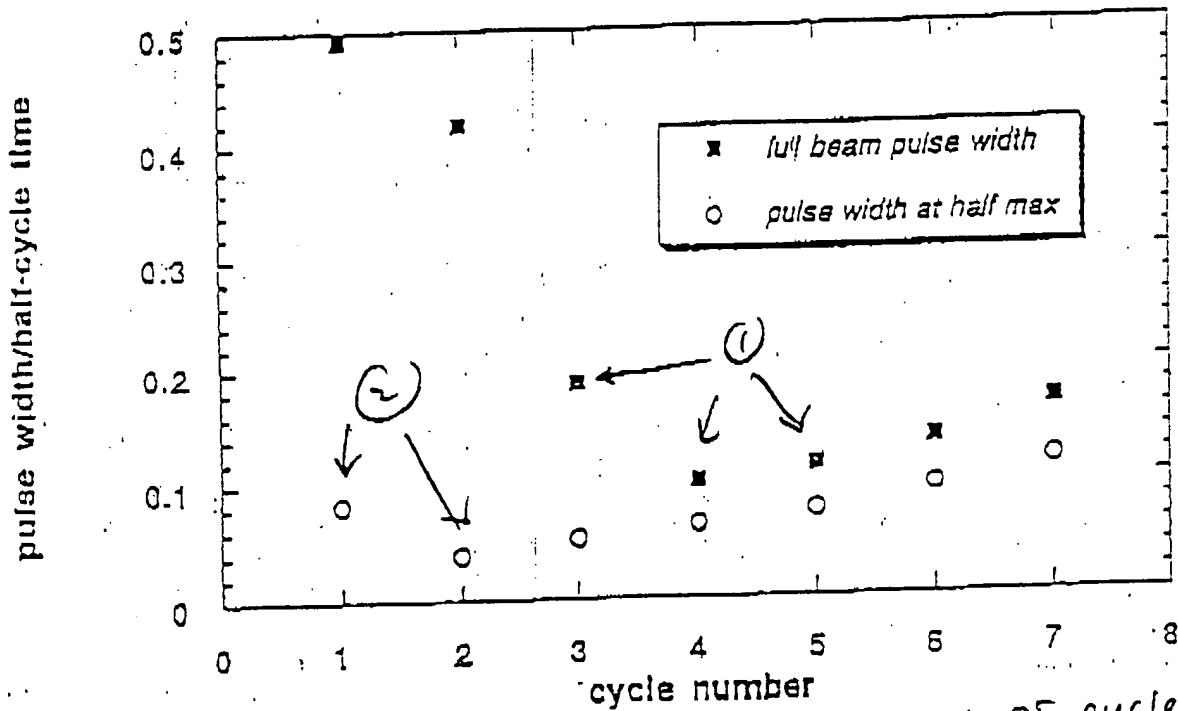


RECEIVED

JUL 01 2004

TECH CENTER 2800

1.3 GHz pulse widths normalized to rf half-cycle time



- ① (solid squares) Beam full width at different RF cycle
② (open circles) Beam full width at half maximum at different RF cycle.

Figure 14: Micro-pulse width (as a fraction of the half-cycle) vs. rf cycle number near the output grid. The full beam pulse width decreases with time, and reaches a minimum at the fourth rf cycle. After saturation there is a slight increase in pulse-width due to space-charge effects.

SUBSTITUTE FIGURE



RECEIVED

JUL 01 2004

TECH CENTER 2800

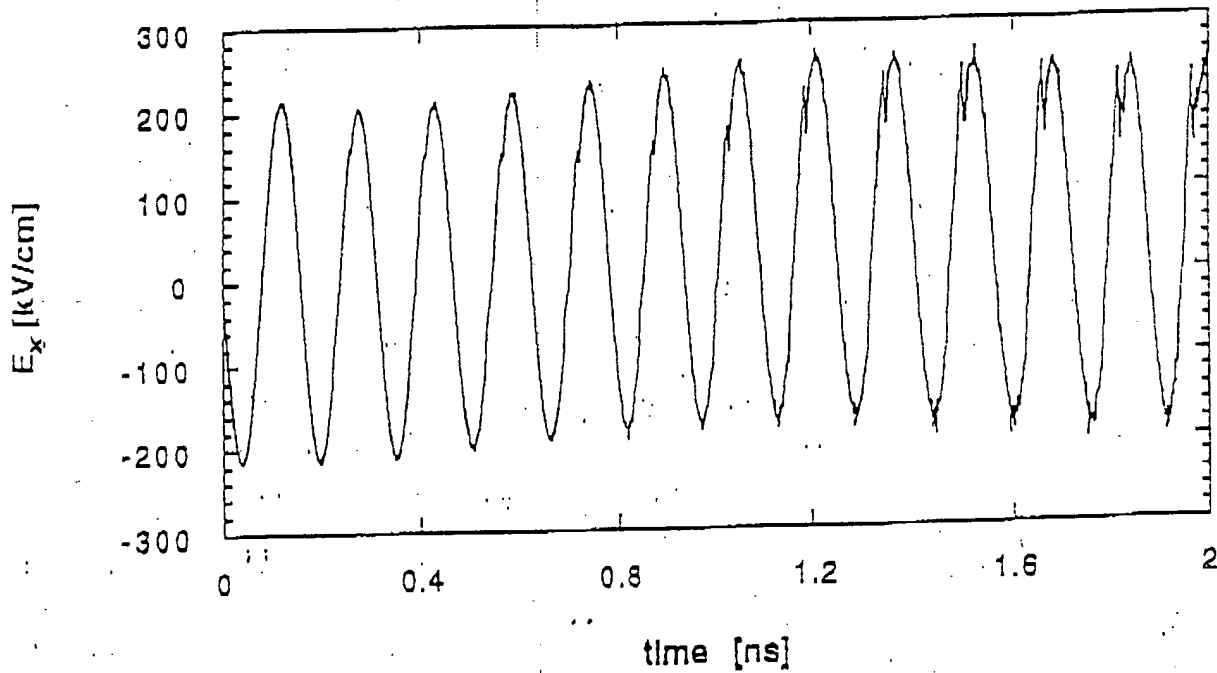


Figure 15: Longitudinal electric field in kv/cm as measured by a probe near the exit grid for the 6.4 GHz, 105 kV simulation.



RECEIVED

JUL 01 2004

TECH CENTER 2800

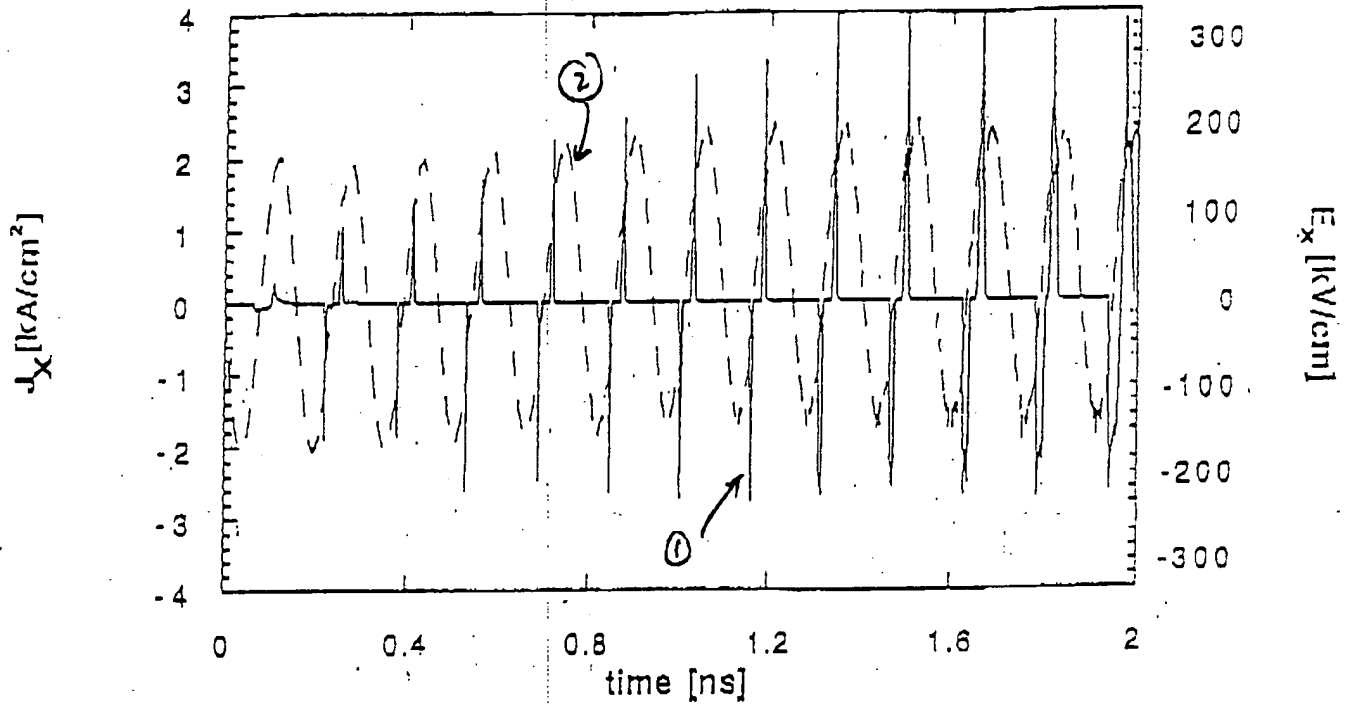


Figure 16: Plot of the current density in kA/cm^2 [solid line] and the longitudinal electric field [dashed line] for the 6.4 GHz, 105 kV simulation.

SUBSTITUTE Figure



RECEIVED

JUL 01 2004

TECH CENTER 2800

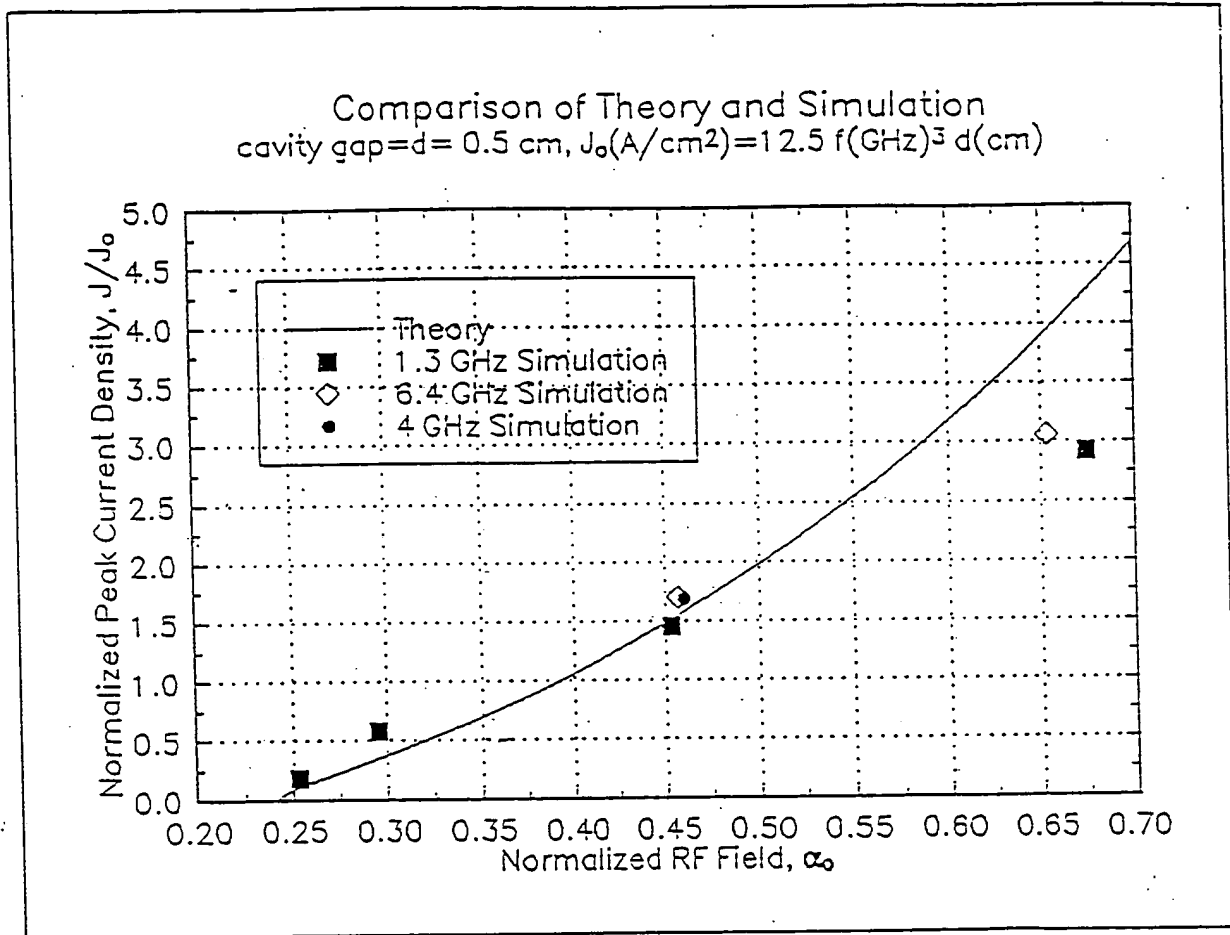


Figure 17: Resonant Tuning Curve (both simulation and theory) showing the tolerance of the micropulse electron gun.



RECEIVED

JUL 01 2004

TECH CENTER 2800

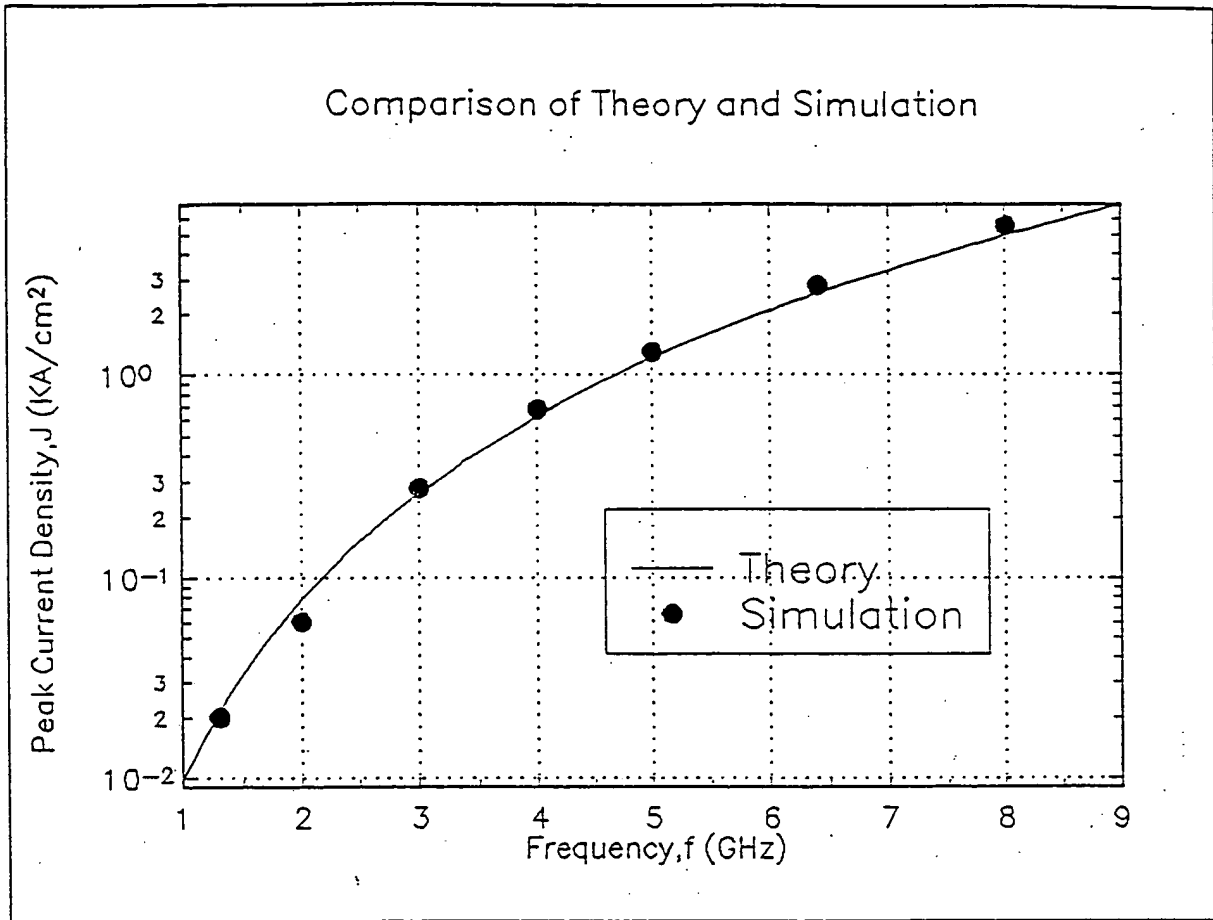


Figure 18: Comparison of peak current density in kA/cm² versus frequency for simulation and theory for a gap length of 0.5 cm and drive parameter $\alpha_0 = 0.453$.



RECEIVED

JUL 01 2004

TECH CENTER 2800

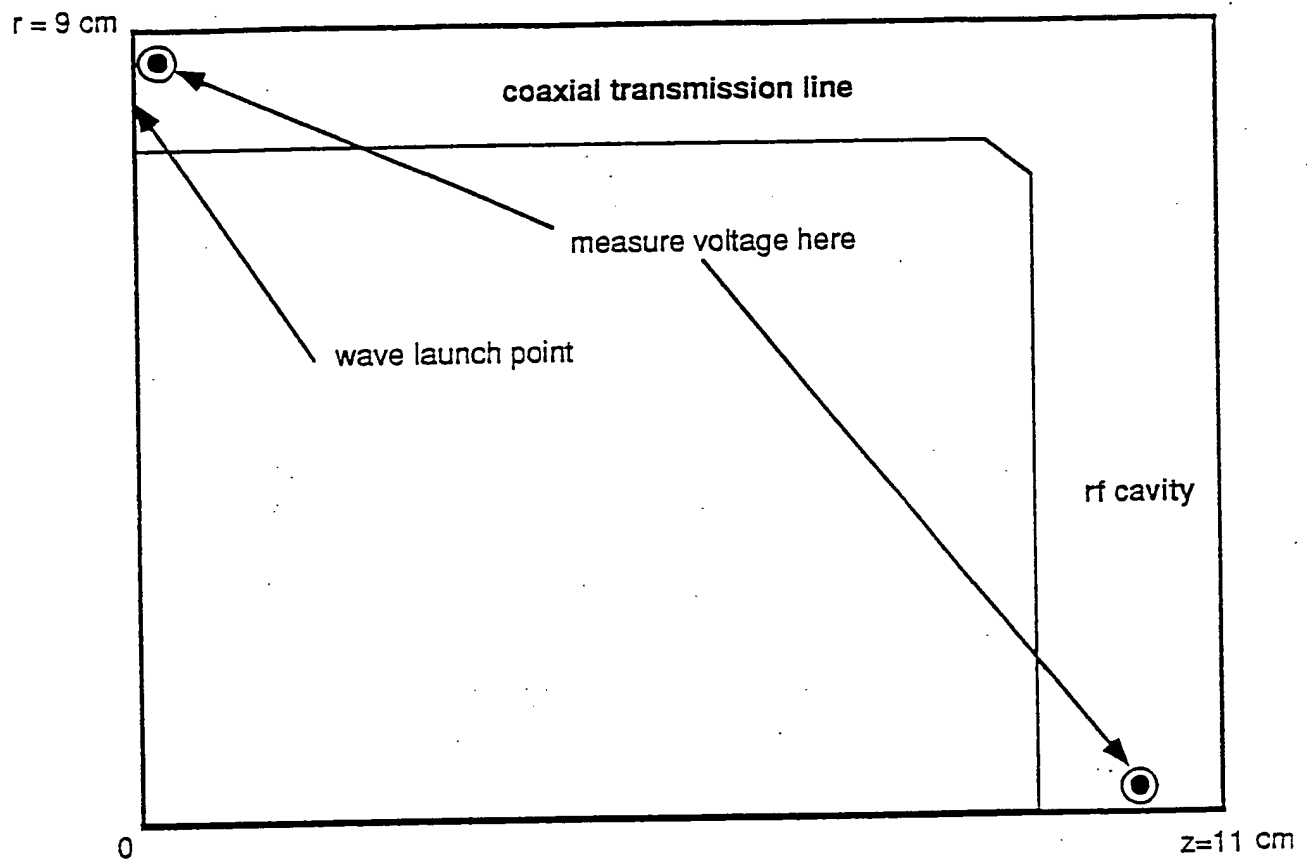


Figure 19: Side view of a cylindrically symmetric coaxial transmission line and cavity. An rf wave is launched at the left end of the coaxial line.



RECEIVED

JUL 01 2004

TECH CENTER 2800

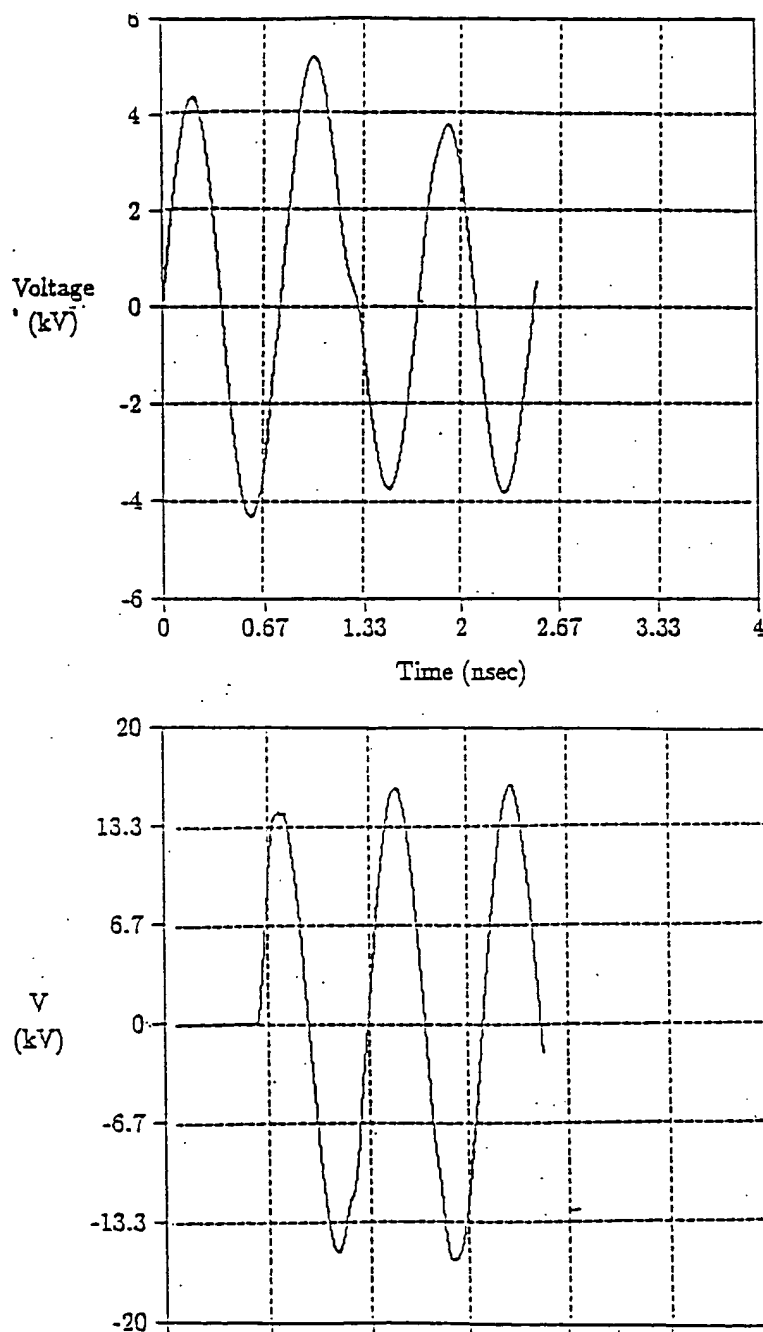


Figure 20: Resulting voltages for a TM_{010} cavity at 1.275 GHz (9 cm radius) with a one cm cavity gap and one cm coaxial gap. (top) voltage measured at entrance of coax, and (bottom) voltage measured at cavity center.



RECEIVED

JUL 01 2004

TECH CENTER 2800

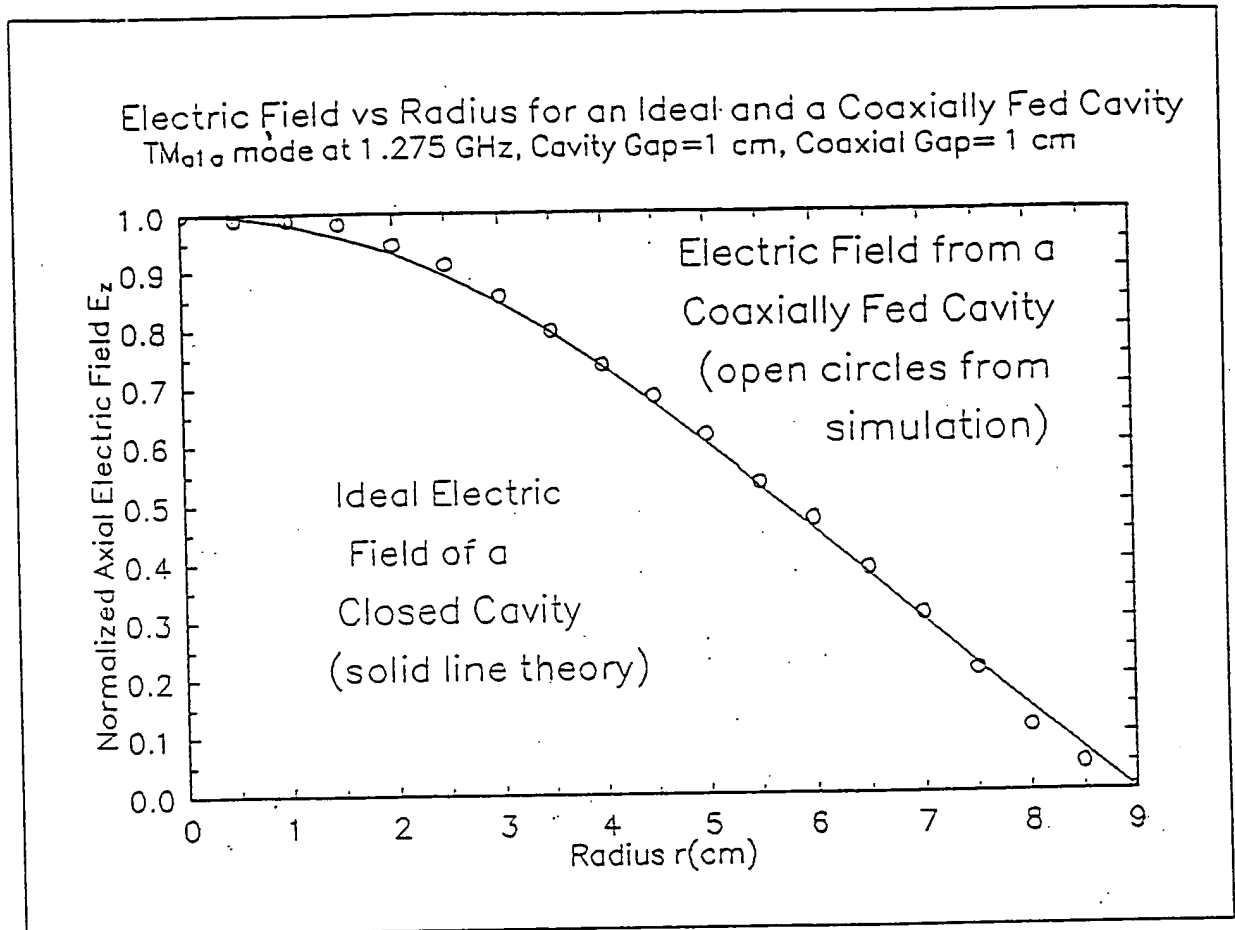


Figure 21: Electric field from a coaxially fed cavity (TM_{010} mode) showing simulation values (open circles) and theoretical curve for an ideal closed cavity.



RECEIVED

JUL 01 2004

TECH CENTER 2800

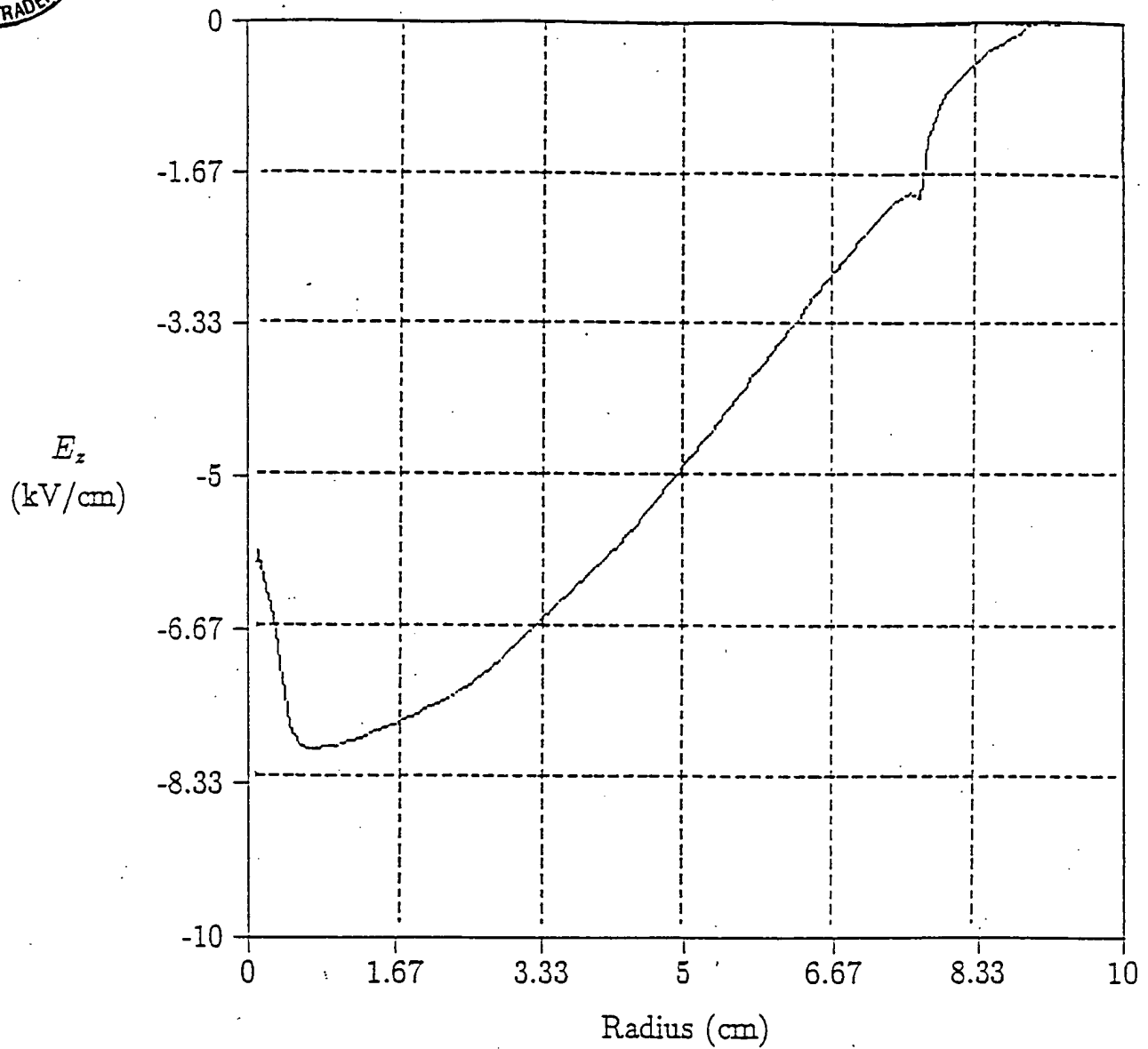


Figure 22: Axial electric field in cavity with a one cm diameter, 40 amp/cm², 25 ps long beam emitted into the cavity. The curve is inverted compared to the plot of Fig. 21. However, the depression at $R = 0$ cm due to space charge is clearly seen. Beam loading reduces the field by about 1/3.



RECEIVED

JUL 01 2004

TECH CENTER 2800

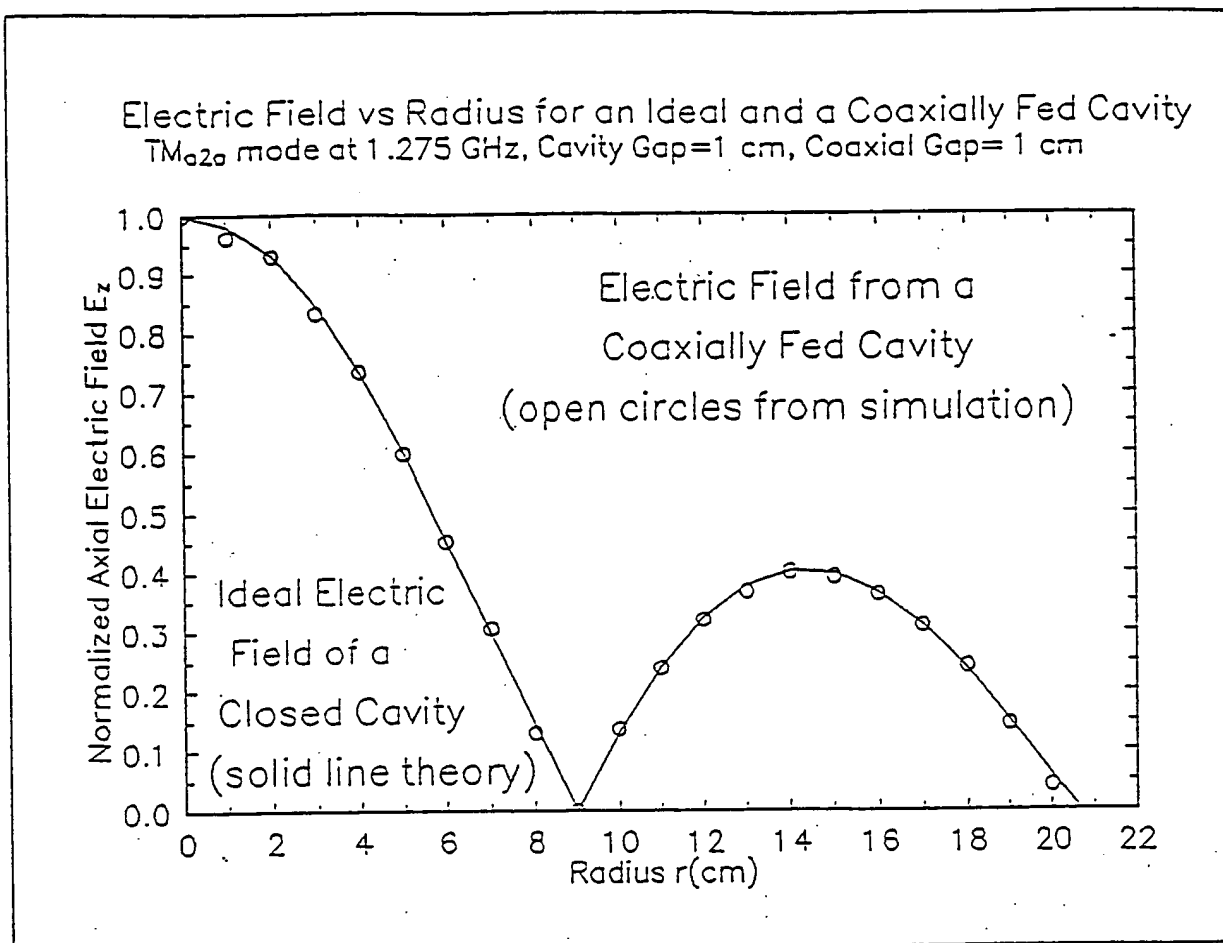


Figure 23: Electric field from a coaxially fed cavity (TM_{020} mode) showing simulation values (open circles) and theoretical curve for an ideal closed cavity.



RECEIVED
JUL 01 2004
TECH CENTER 2800

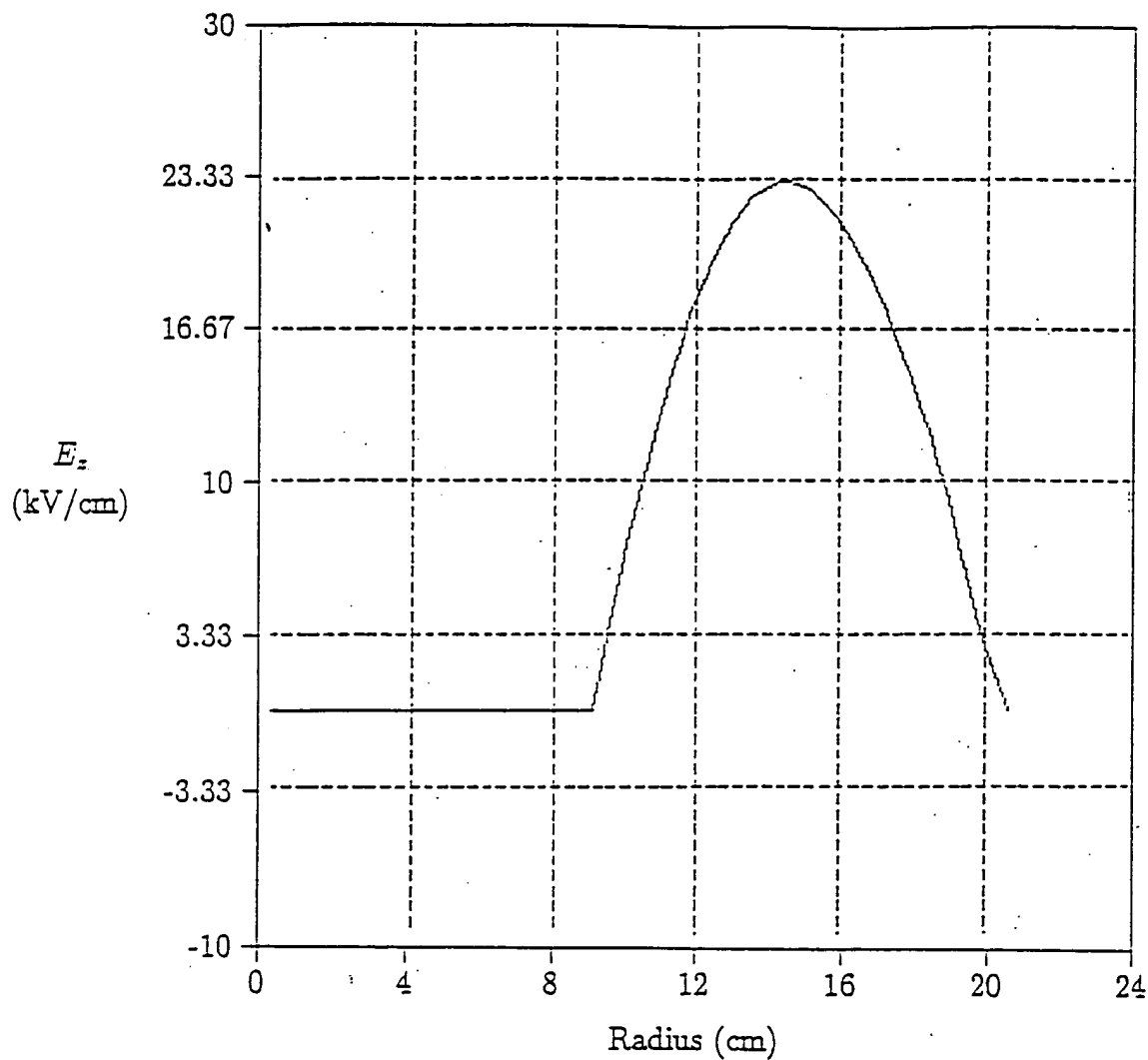


Figure 24: Axial electric field vs. radius from a coaxially fed cavity (TM_{020} mode (simulation) with inner conductor at first zero of the mode. The first peak has clearly been eliminated. Frequency 1.275 GHz and one cm gap.



RECEIVED

JUL 01 2004

TECH CENTER 2800

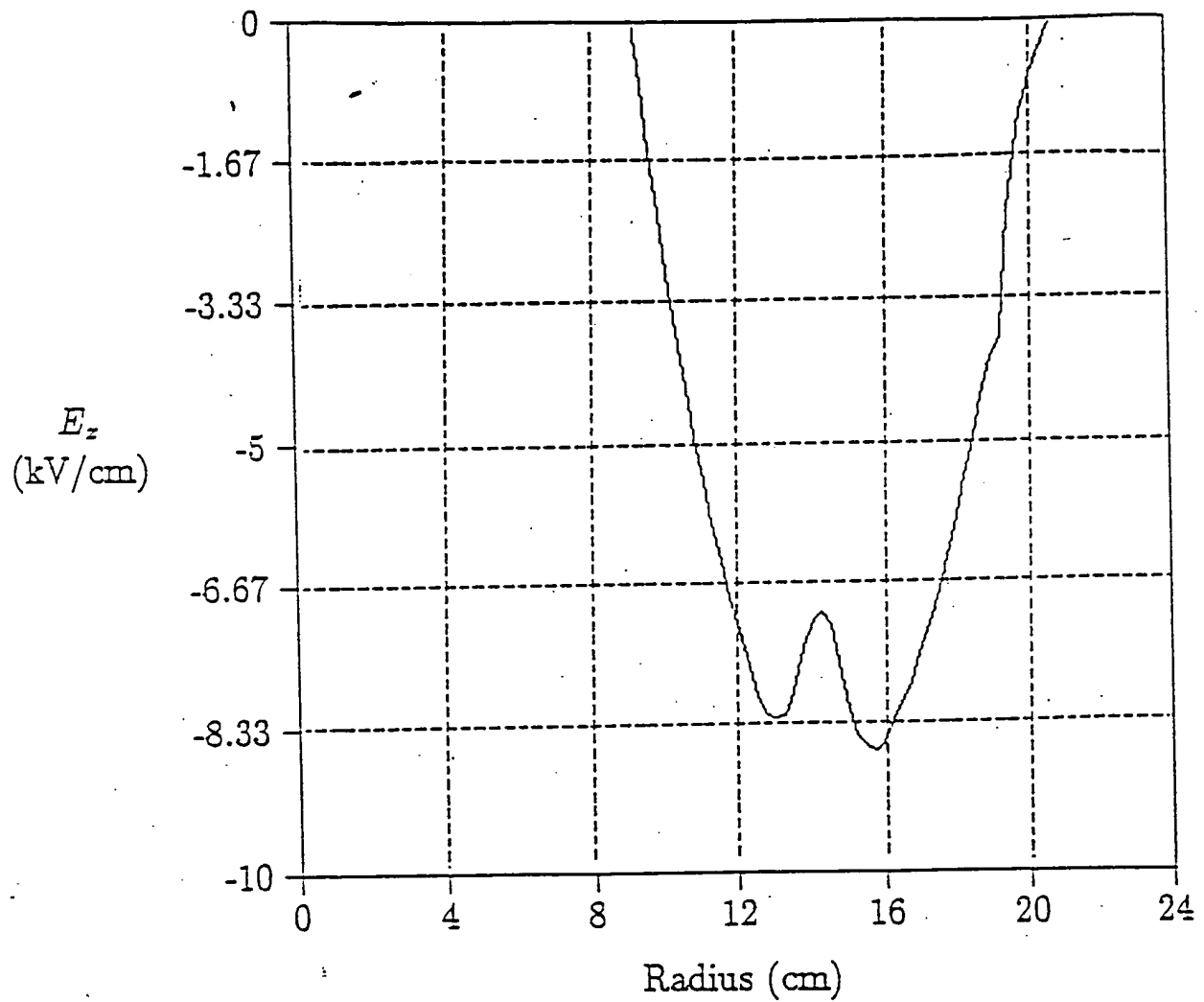


Figure 25: Axial electric field as a function of radius loaded down by a 40 amp/cm², 25 ps pulse, and one cm diameter electron beam. The curve is inverted compared to the plot of Fig. 24. However, the depression at $R \approx 14$ cm due to space charge is clearly seen.



RECEIVED

JUL 01 2004

TECH CENTER 2800

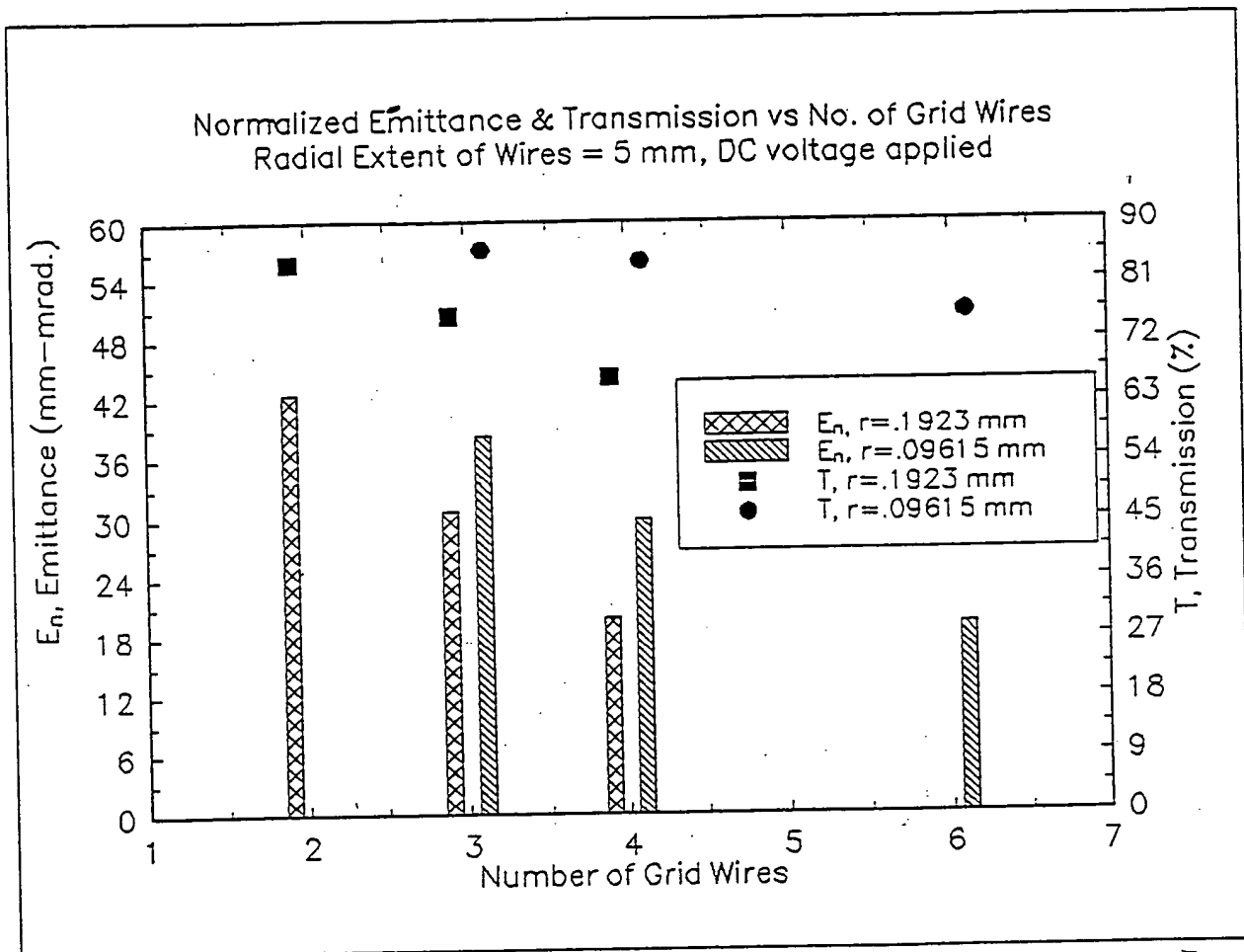


Figure 26: Normalized emittance and transmission versus number of grid wires with a dc voltage applied to the cavity.



RECEIVED

JUL 01 2004

TECH CENTER 2800

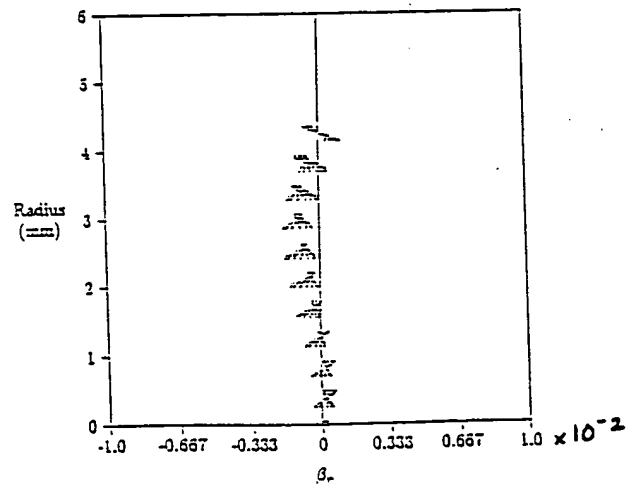
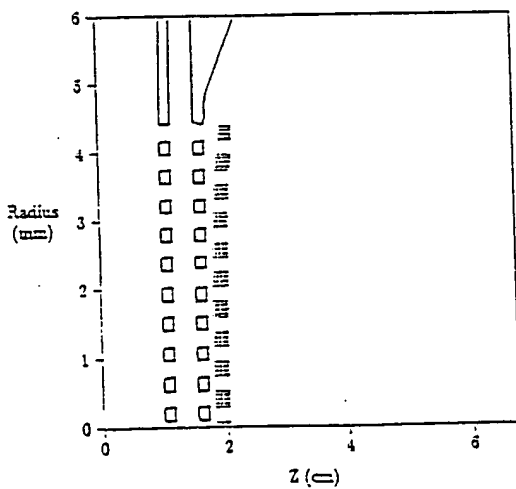
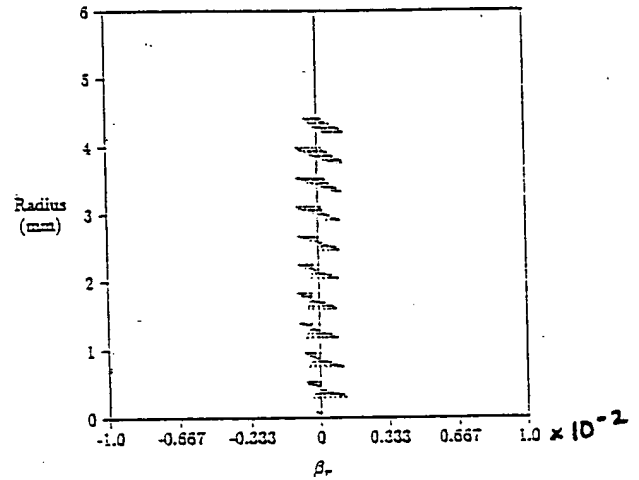
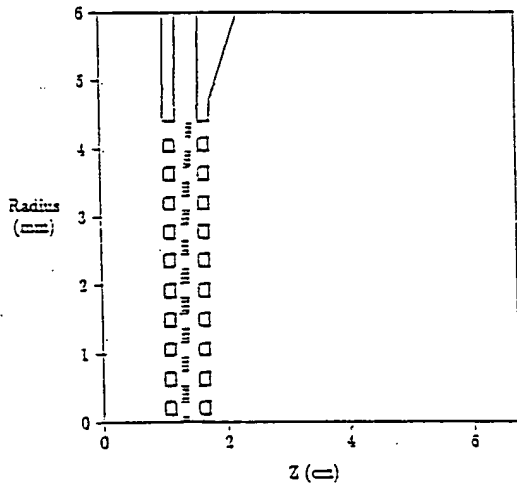
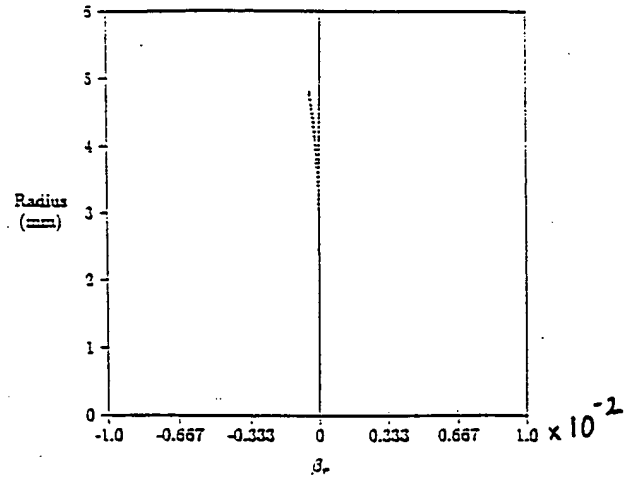
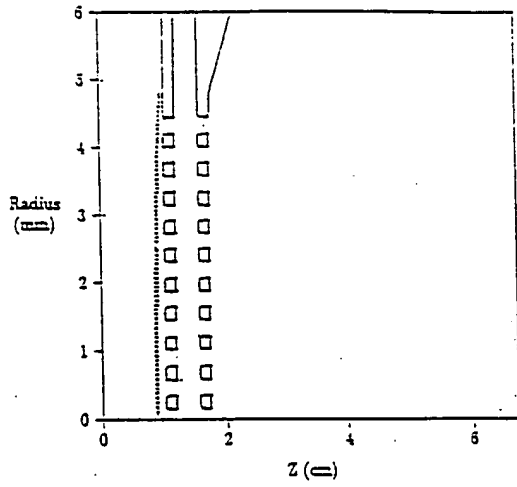


Figure 27: Configuration space and phase space for a solid beam from the simulations. This shows the emittance growth up to the first grid, from the first grid, and from the second grid.



RECEIVED

JUL 01 2004

TECH CENTER 2800

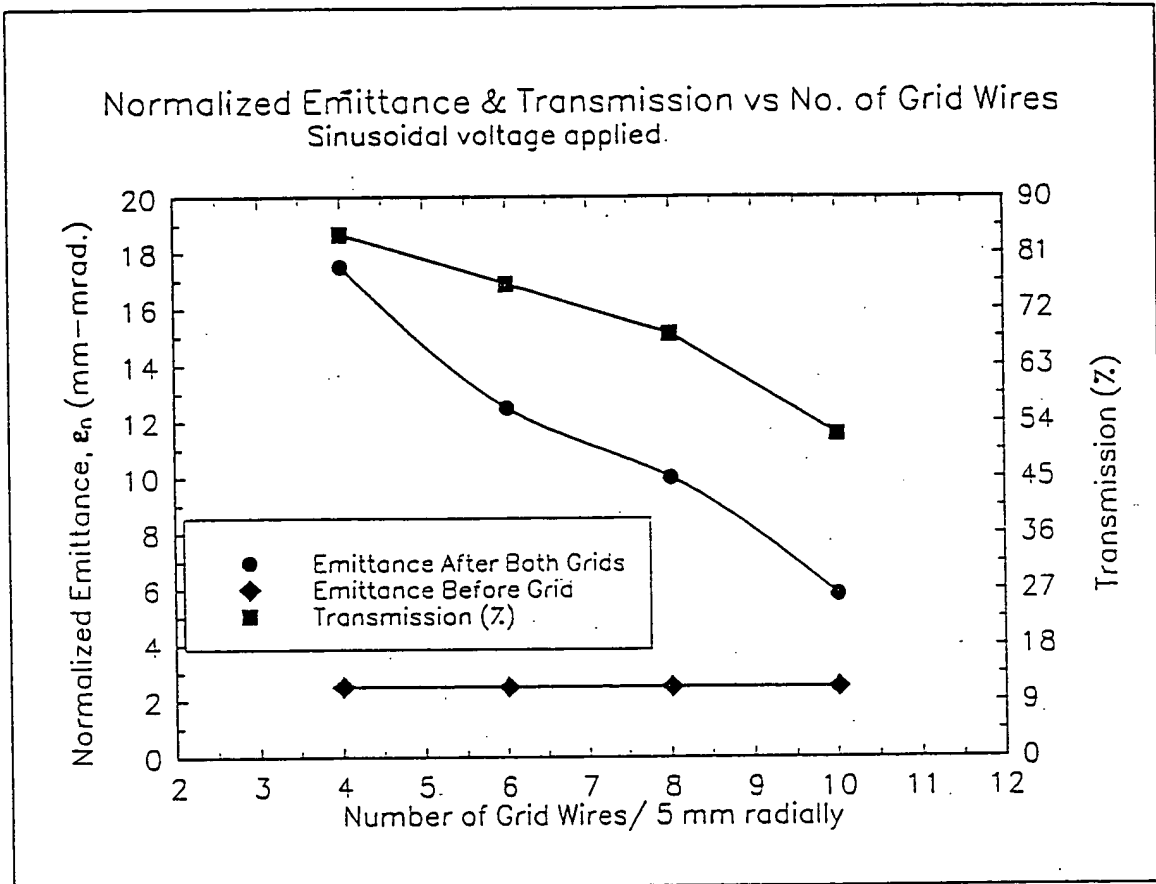


Figure 28: Normalized emittance and transmission versus number of grid wires with an *ac* voltage applied to the cavity. Grid wire radius is 0.09615 mm.



RECEIVED

JUL 01 2004

TECH CENTER 2800

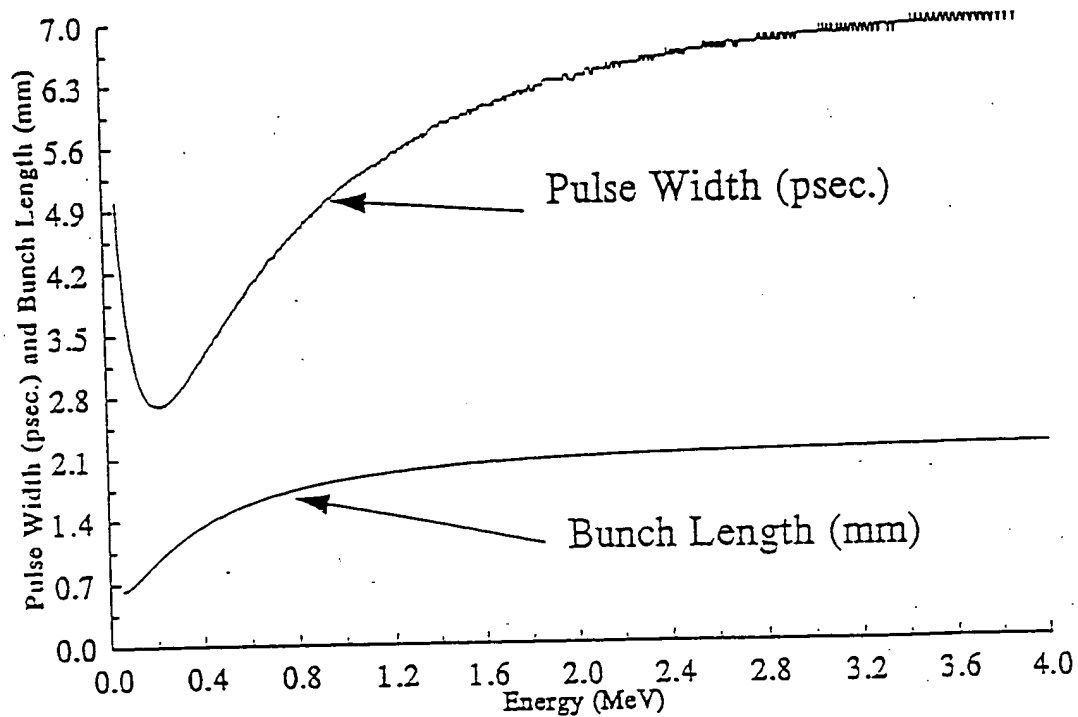


Figure 29: Expansion of micro-pulse from space charge during acceleration, neglecting energy spread. The acceleration field is 20 MV/m and the axial space charge electric field is 2.9 MV/m (corresponding to about 100 nC/cm³). The initial pulse width is 5 ps at an initial energy of 50 keV.



RECEIVED

JUL 01 2004

TECH CENTER 2800

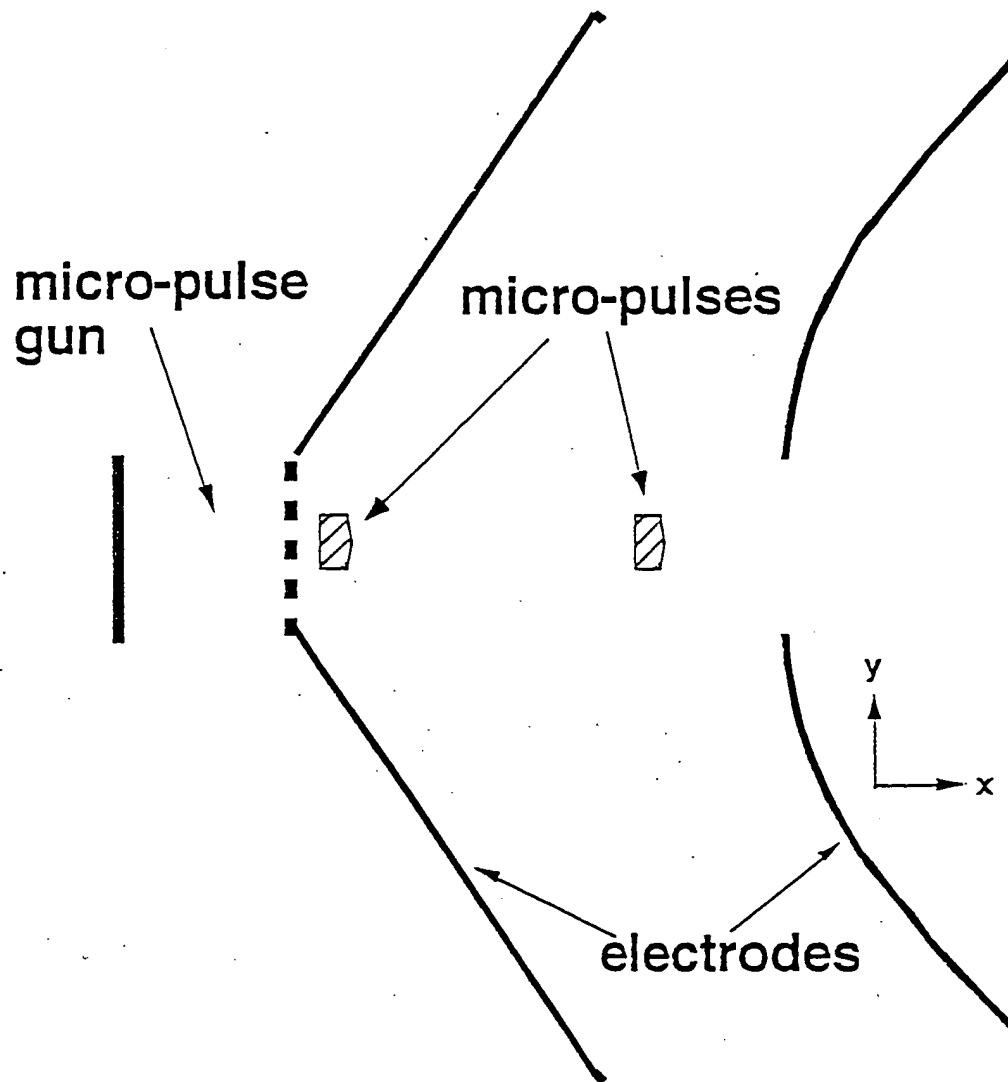


Figure 30: Schematic drawing of a set of electrode shapes for a high-power diode using the modified formulas to the usual Pierce shapes as discussed in the text.



RECEIVED

JUL 01 2004

TECH CENTER 2800

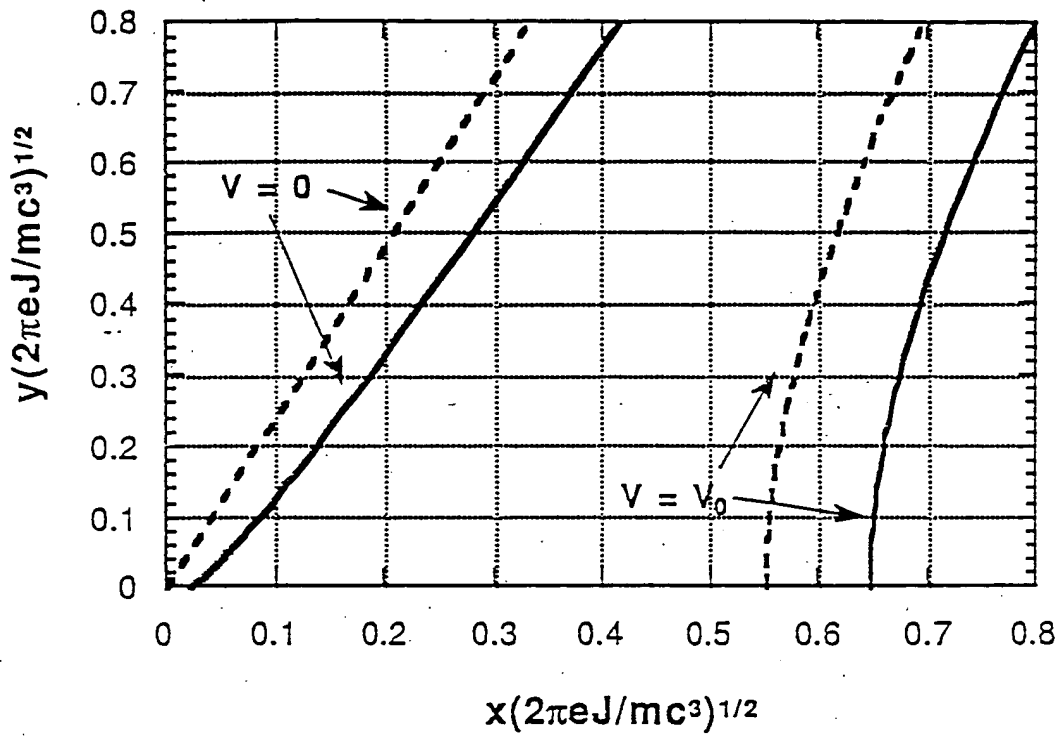


Figure 31: Plot of electrode shapes for a non-space-charge-limited 0.5 MeV diode. The modified shapes [solid lines] and the classical Pierce shapes [broken lines] are shown for comparison. The value of the electric field E_0 at the cathode is such that the quantity $\nu = 2$



RECEIVED

JUL 01 2004

TECH CENTER 2800

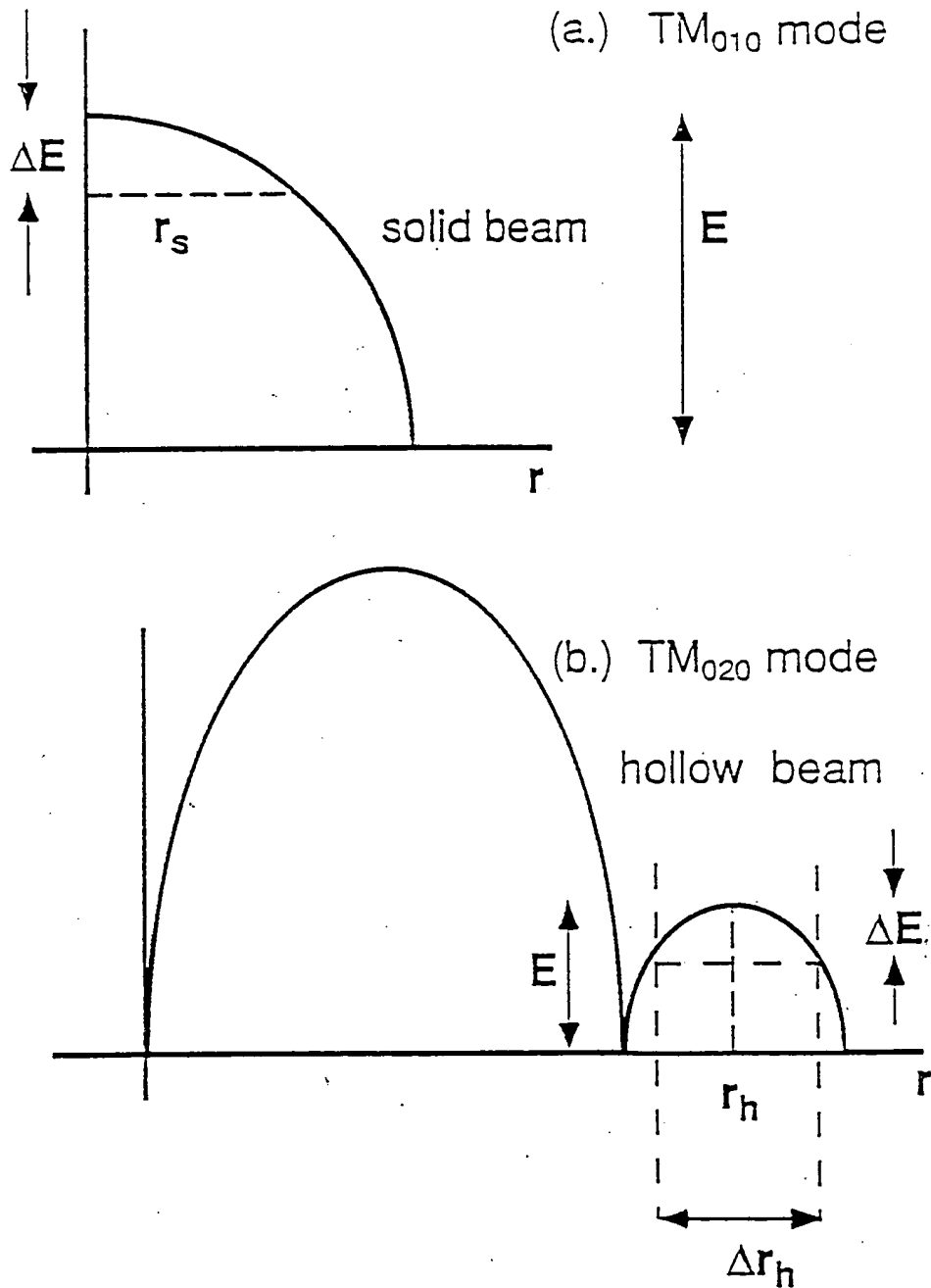


Figure 32: Schematic drawing of emission area and energy spread for a micropulse.



RECEIVED

JUL 01 2004

TECH CENTER 2800

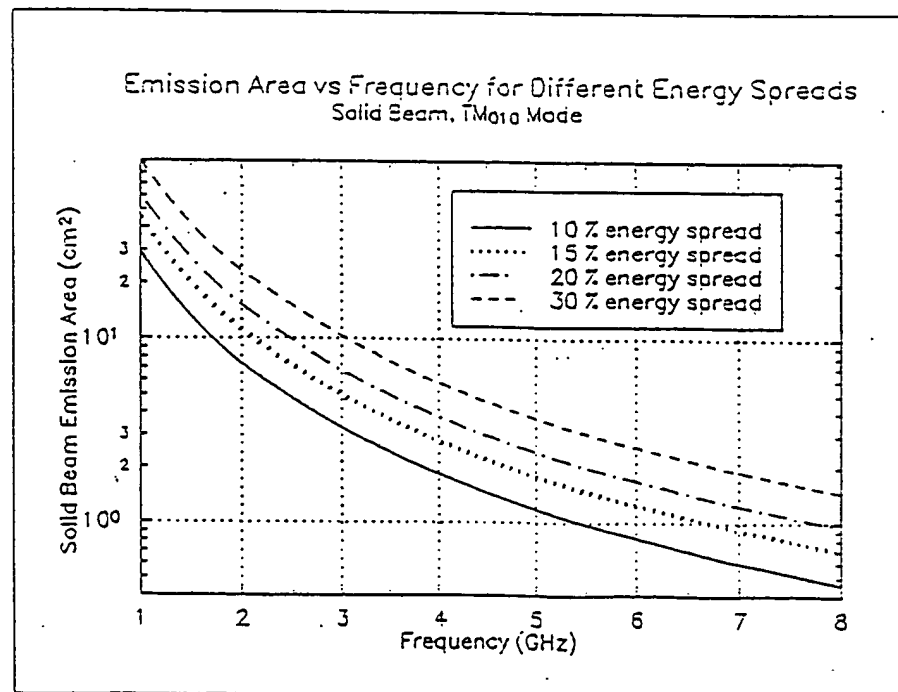
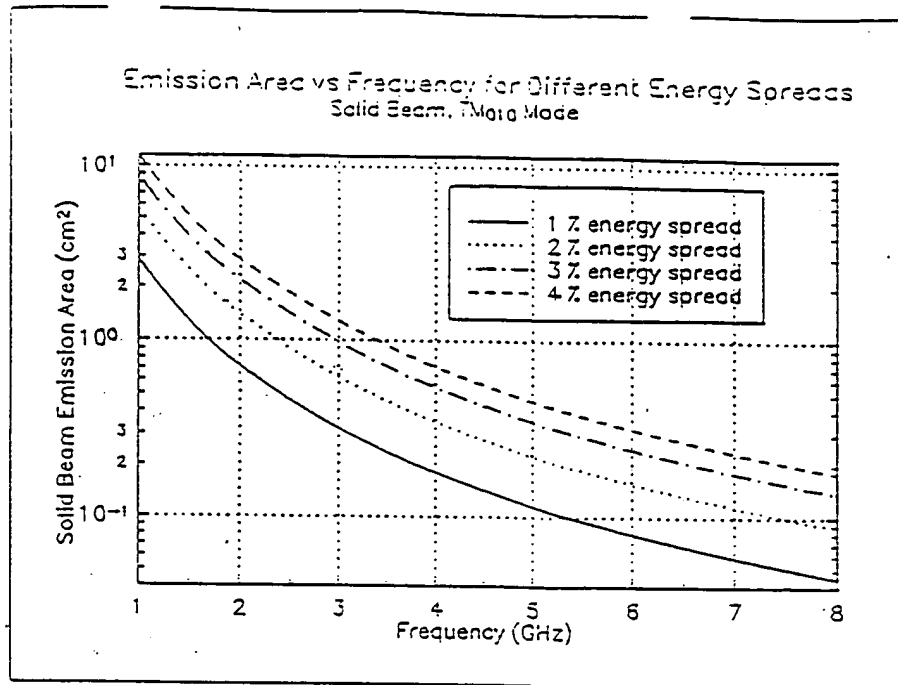


Figure 33: Emission area for a solid beam vs. frequency for different energy spreads (top) 1%-4% energy spread; (bottom) 10%-30% energy spread.



RECEIVED

JUL 01 2004

TECH CENTER 2800

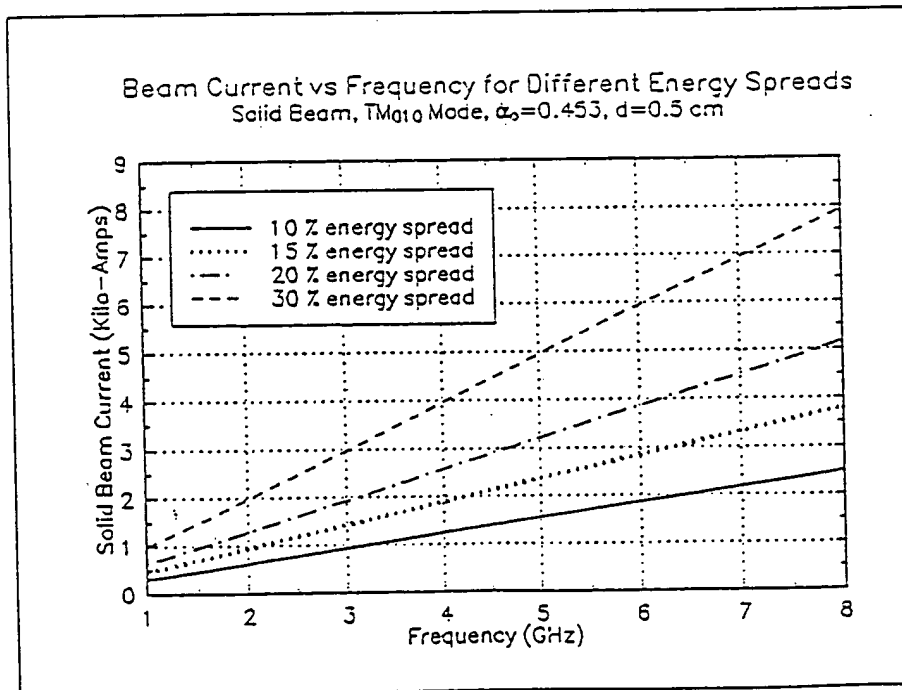
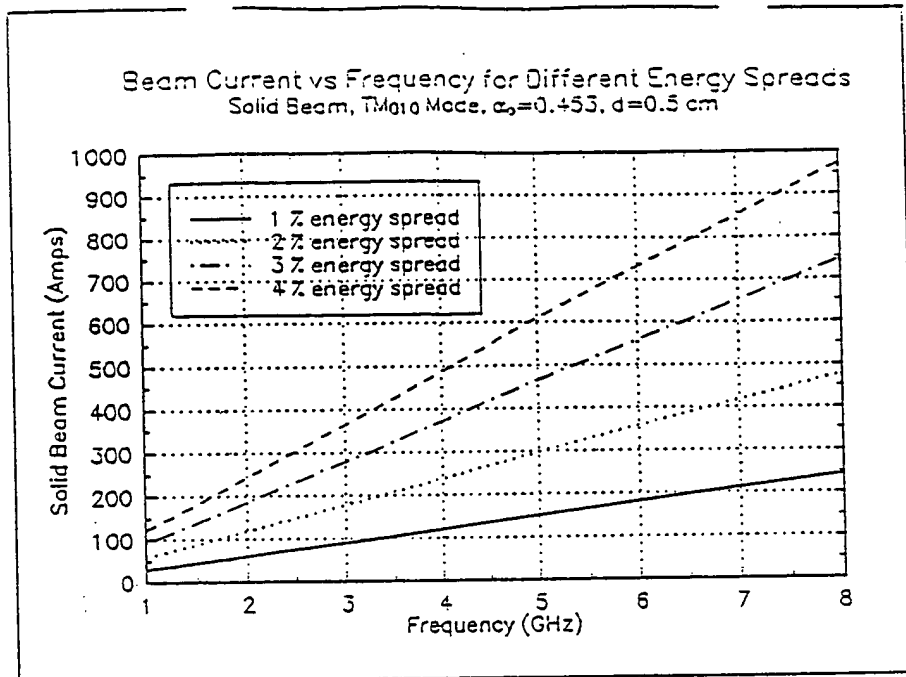


Figure 34: Beam current (solid beam) vs. frequency for different energy spreads and a gap of 0.5 cm.



RECEIVED

JUL 01 2004

TECH CENTER 2800

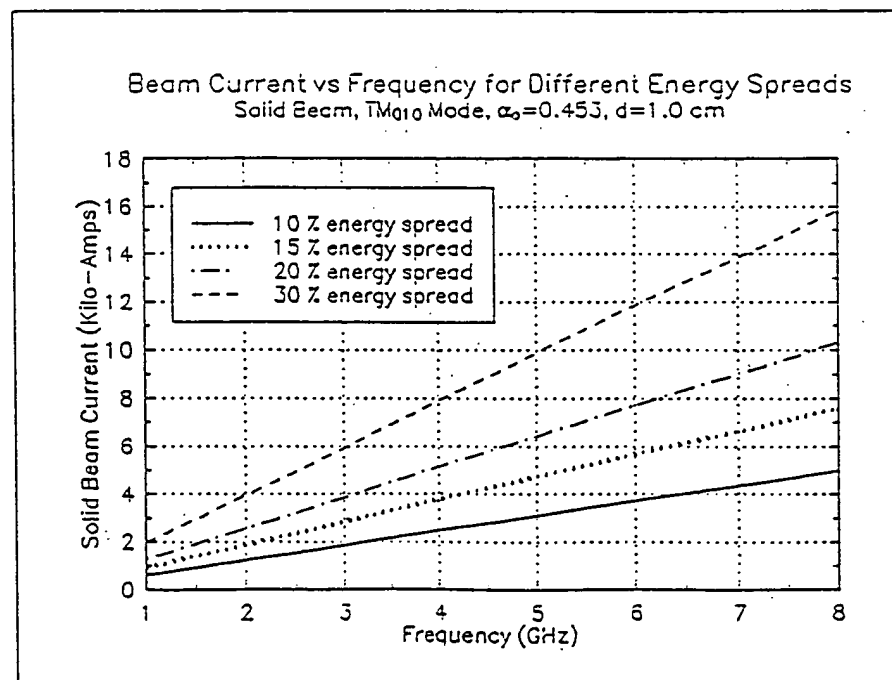
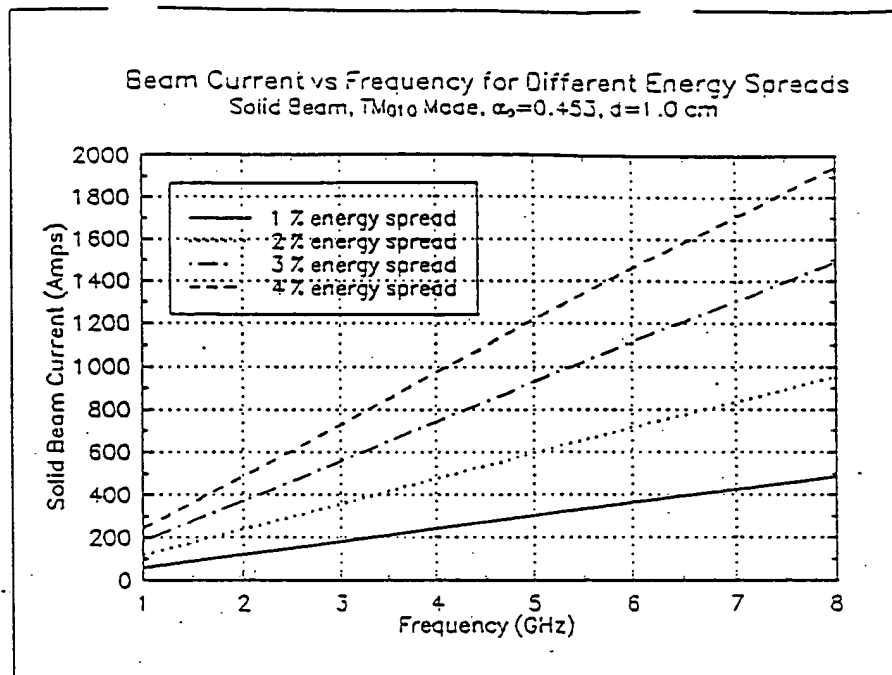


Figure 35: Beam current (solid beam) vs. frequency for different energy spreads and a gap of 1.0 cm.



RECEIVED

JUL 01 2004

TECH CENTER 2800

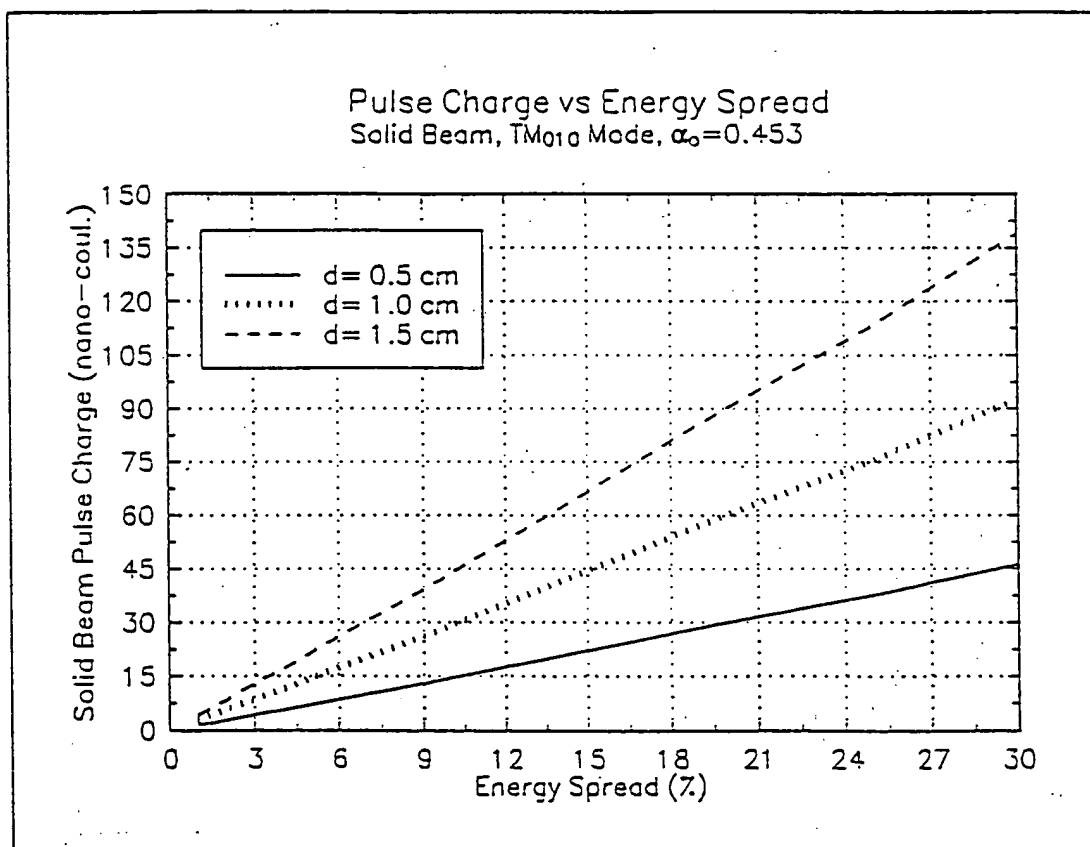


Figure 36: Charge per pulse for a solid beam vs. energy spread.



RECEIVED

JUL 01 2004

TECH CENTER 2800

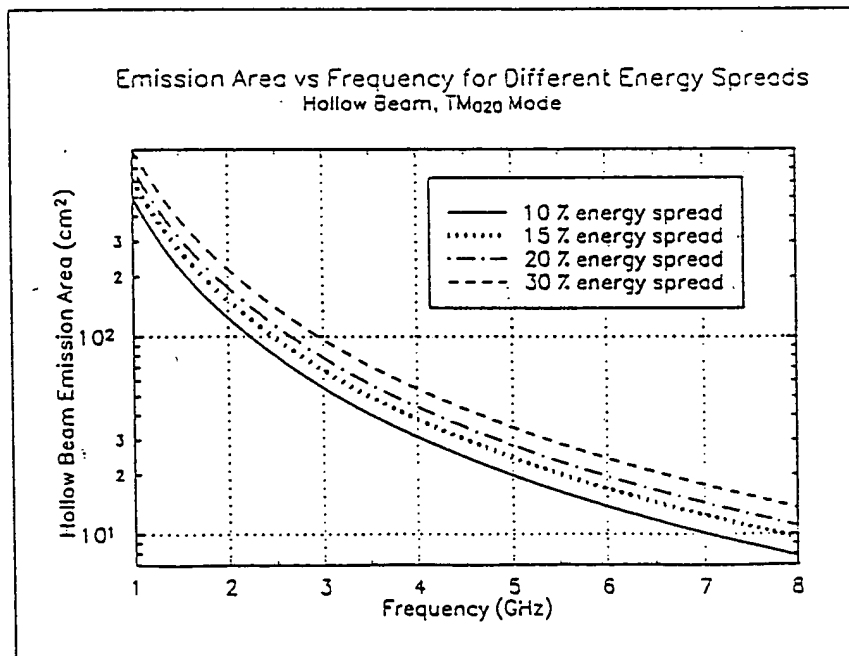
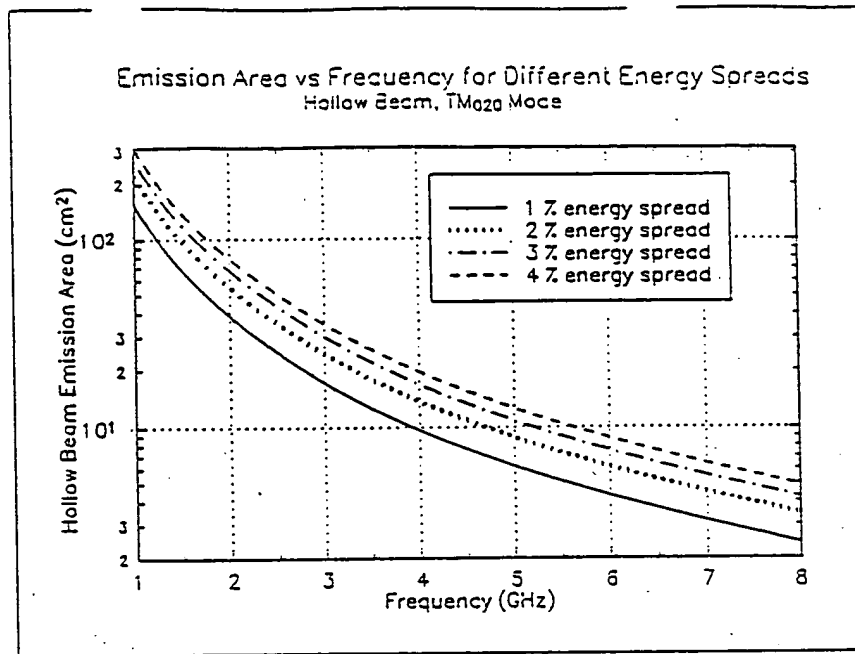


Figure 37: Emission area vs. frequency for different energy spreads. Hollow beam.



RECEIVED

JUL 01 2004

TECH CENTER 2800

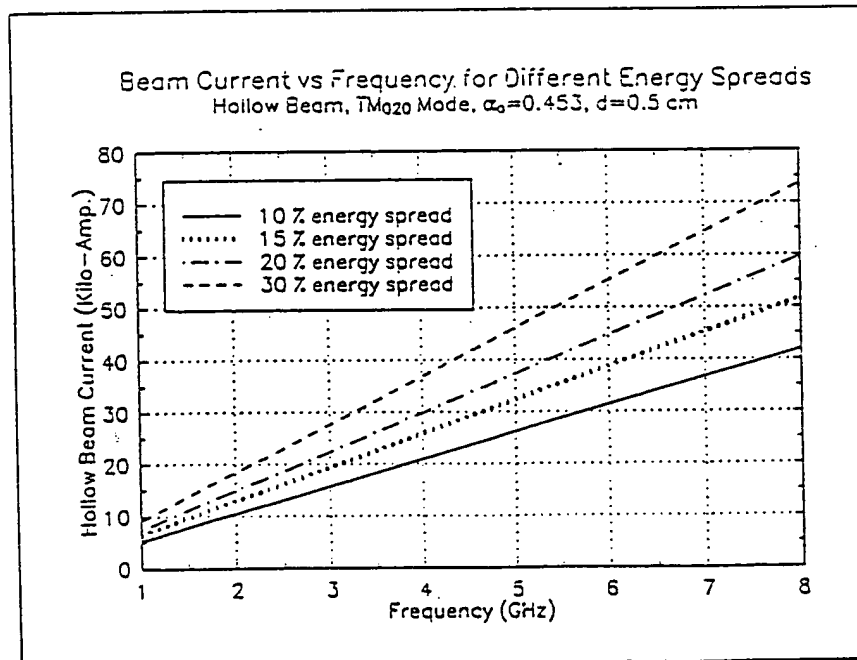
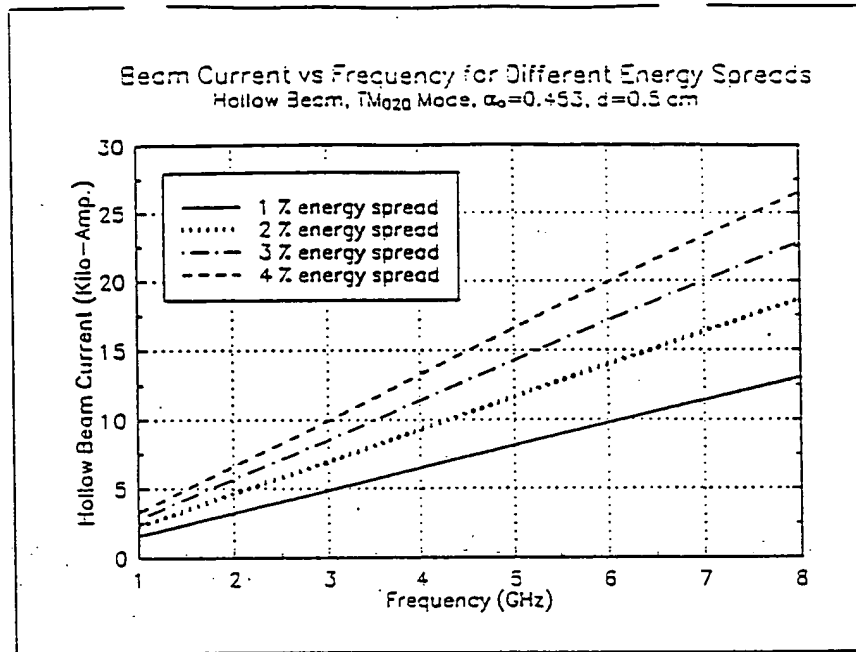


Figure 38: Beam current vs. frequency for different energy spreads. Hollow beam, and $d = 0.5$ cm.



RECEIVED

JUL 01 2004

TECH CENTER 2800

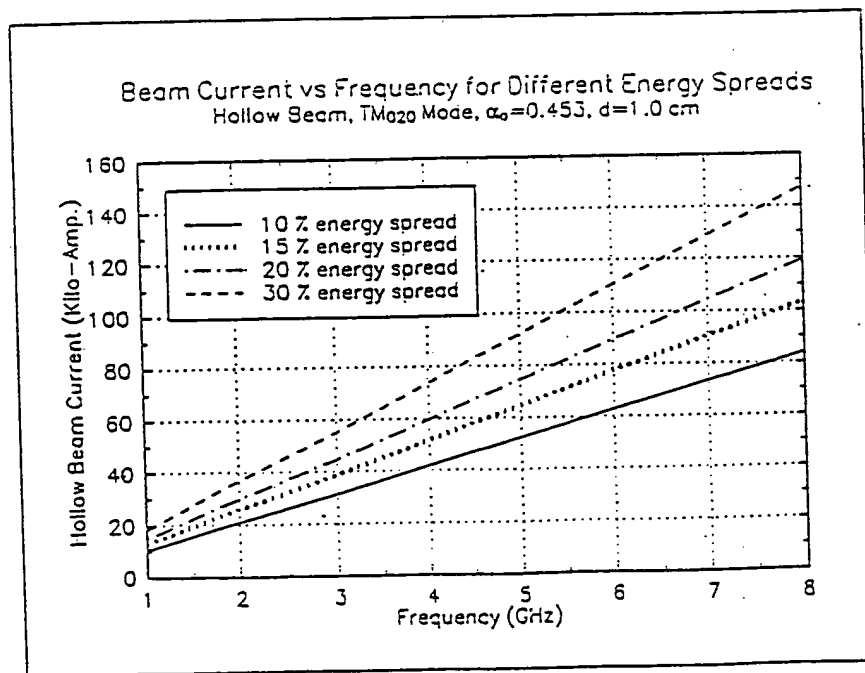
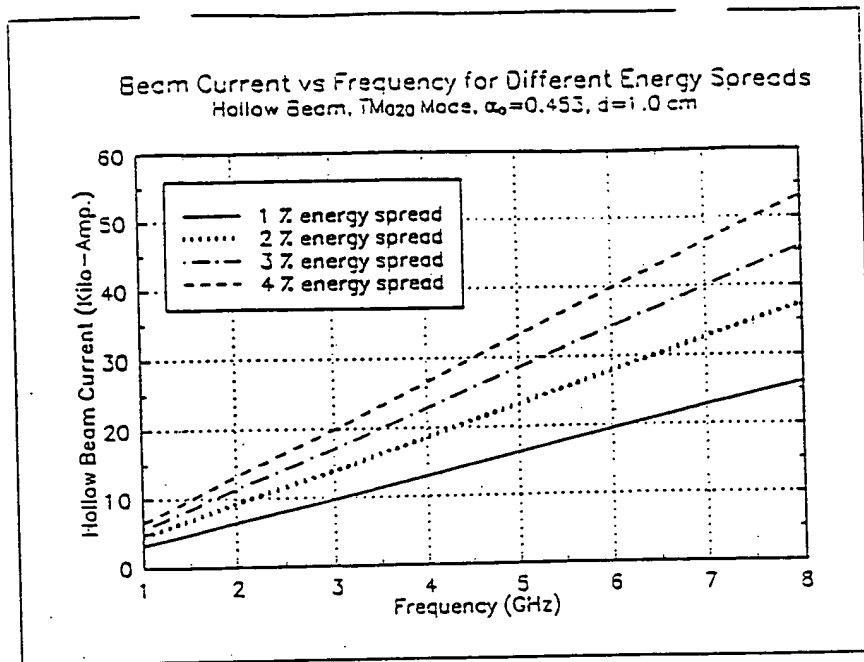


Figure 39: Beam current vs. frequency for different energy spreads. Hollow beam, and $d = 1.0$ cm.



RECEIVED

JUL 01 2004

TECH CENTER 2800

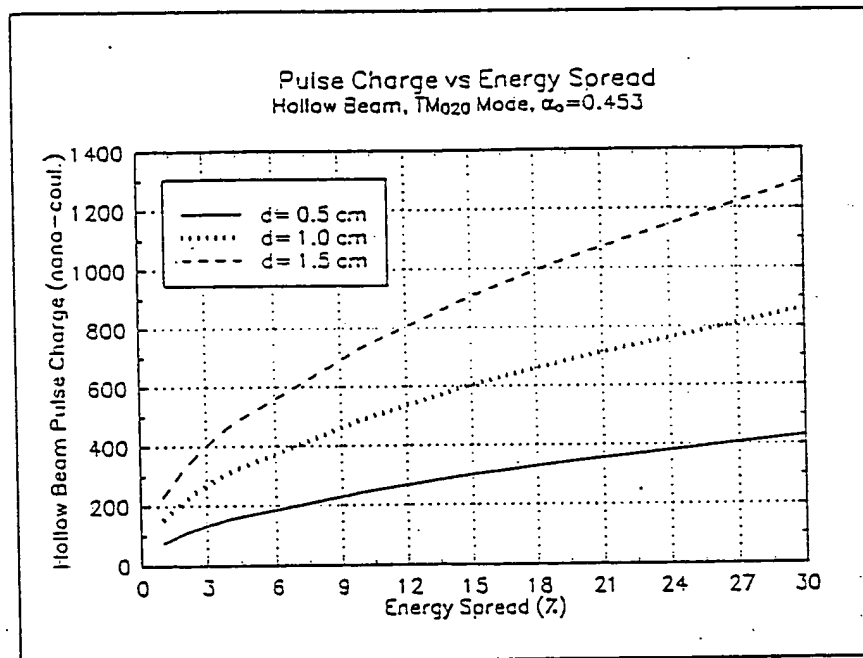


Figure 40: Pulse charge vs. energy spread for hollow beam.



RECEIVED

JUL 01 2004

TECH CENTER 2800

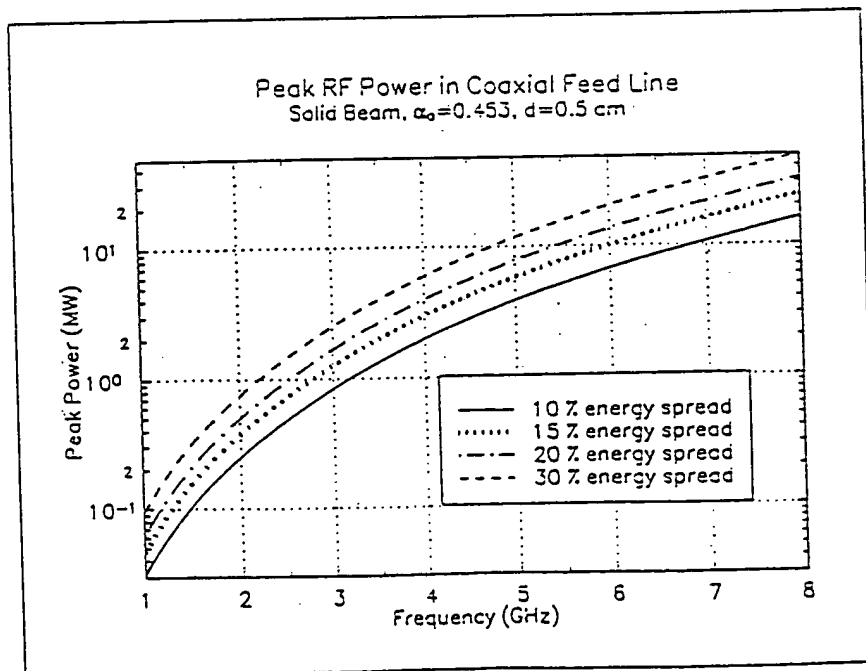
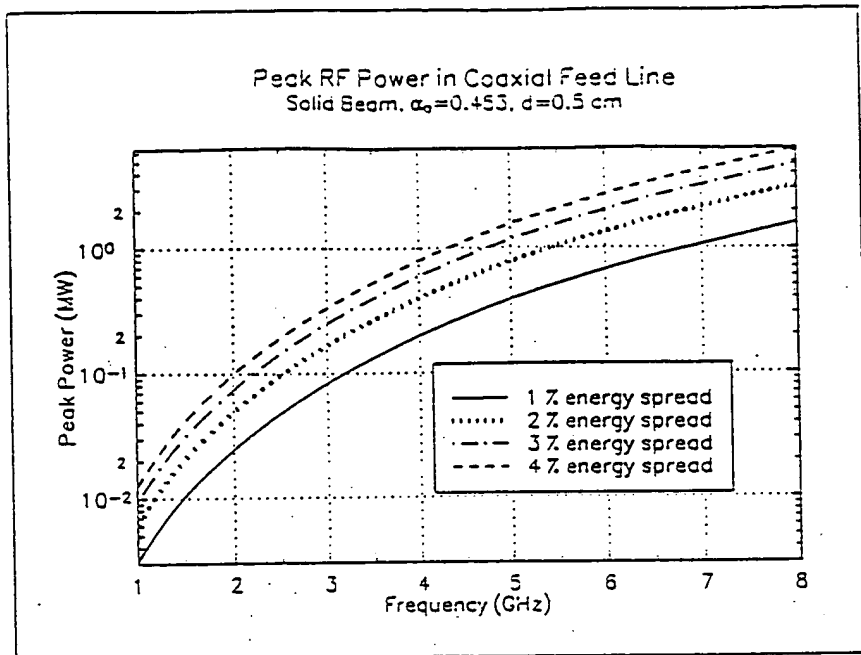


Figure 41: Peak rf power in coaxial feed line for a solid beam, $d = 0.5$ cm.



RECEIVED

JUL 01 2004

TECH CENTER 2800

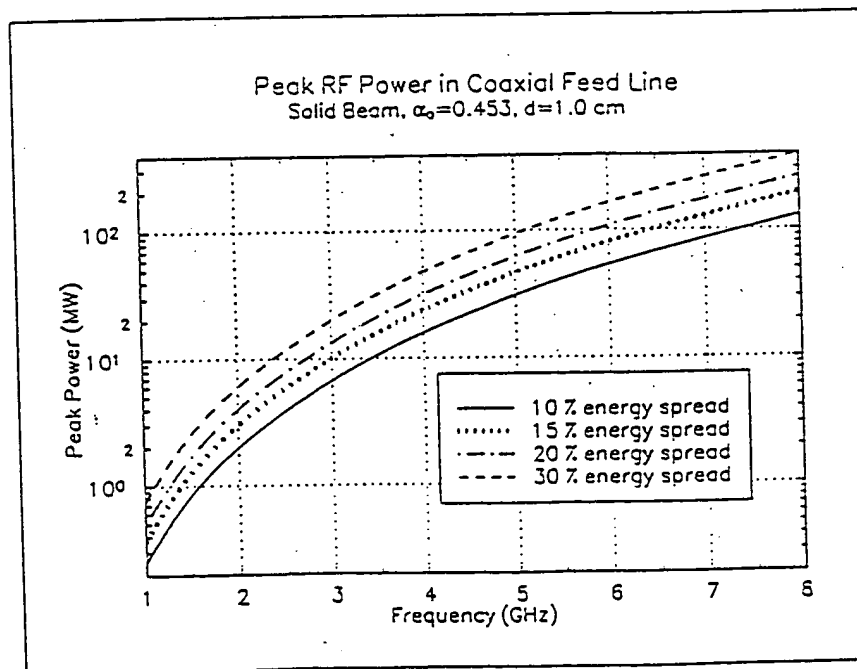
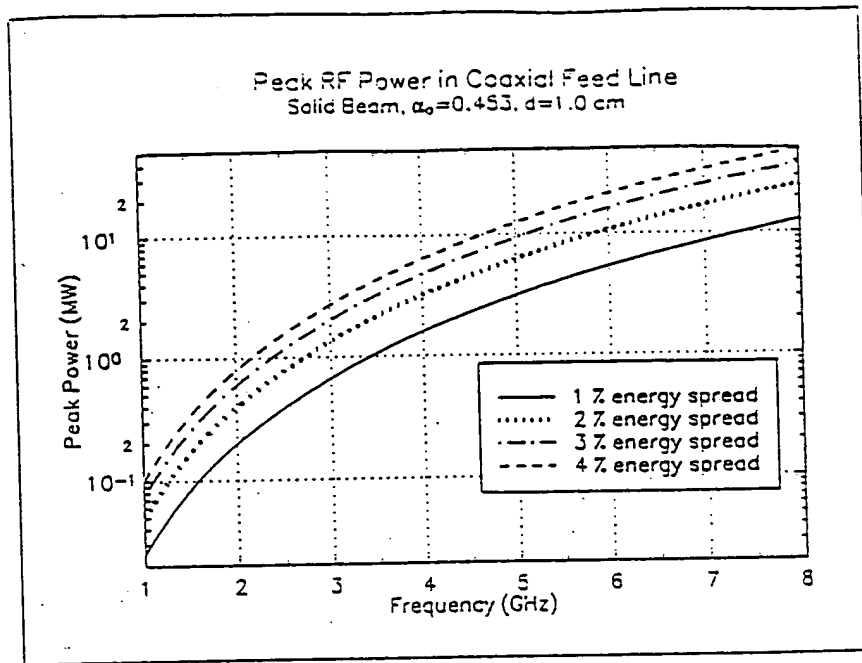


Figure 42: Peak rf power in coaxial feed line for a solid beam, $d = 1.0$ cm.



RECEIVED

JUL 01 2004

TECH CENTER 2800

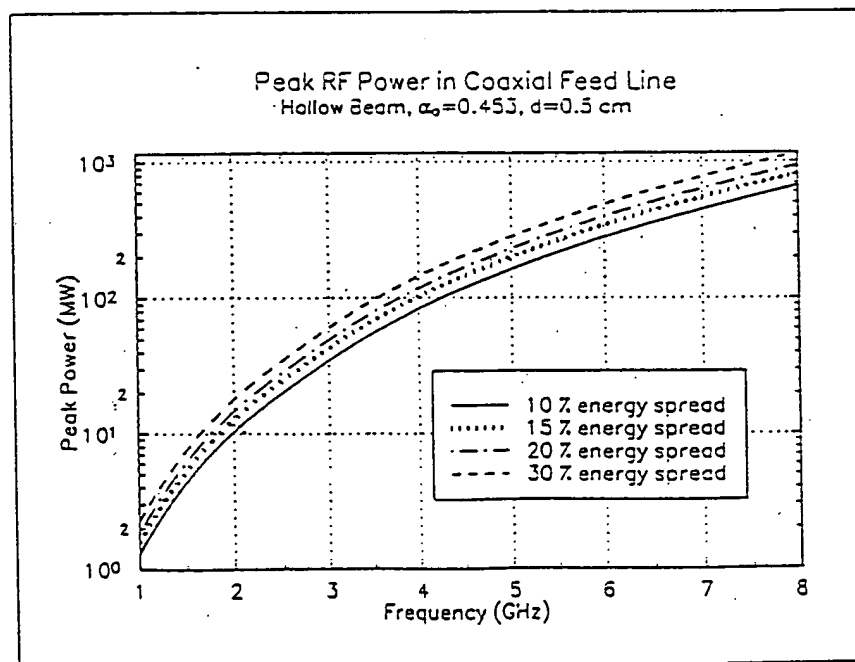
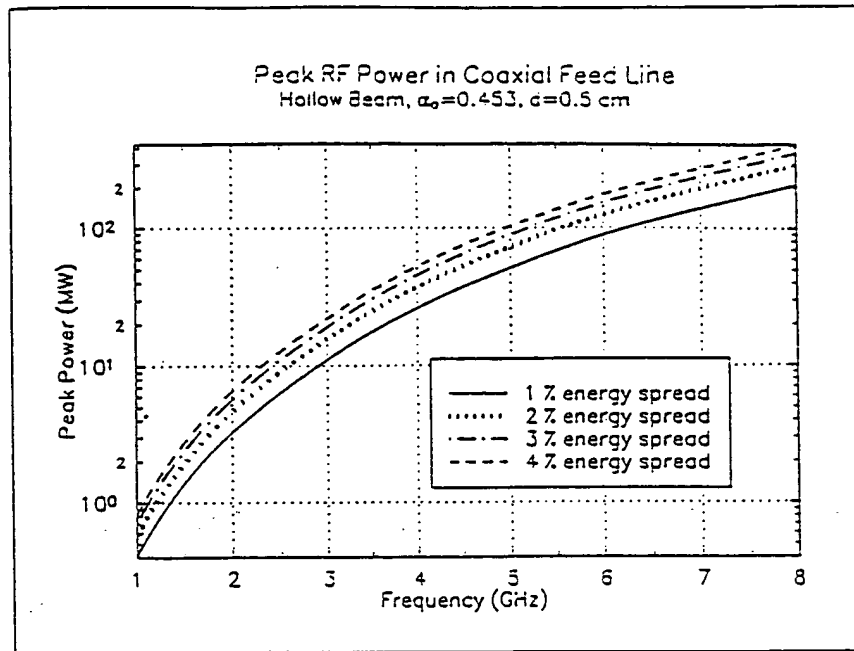


Figure 43: Peak rf power in coaxial feed line for a solid beam, $d = 0.5$ cm.



RECEIVED

JUL 01 2004

TECH CENTER 2800

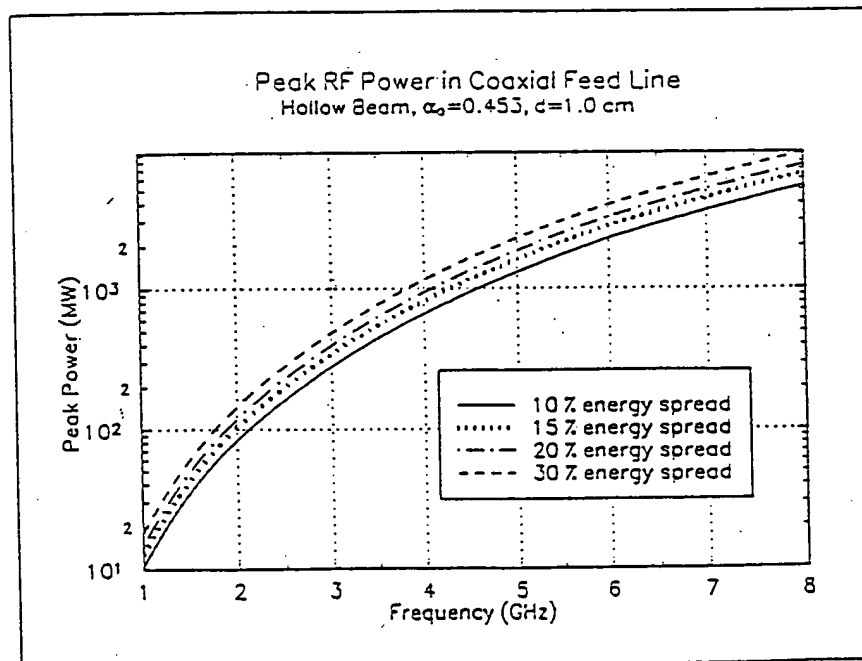
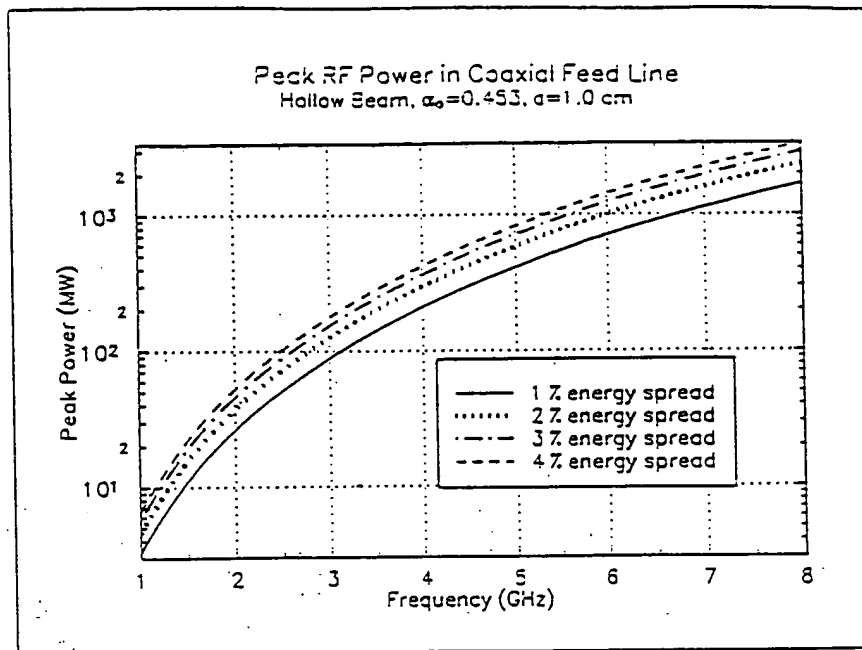


Figure 44: Peak rf power in coaxial feed line for a solid beam, $d = 1.0$ cm.



RECEIVED

JUL 01 2004

TECH CENTER 2800

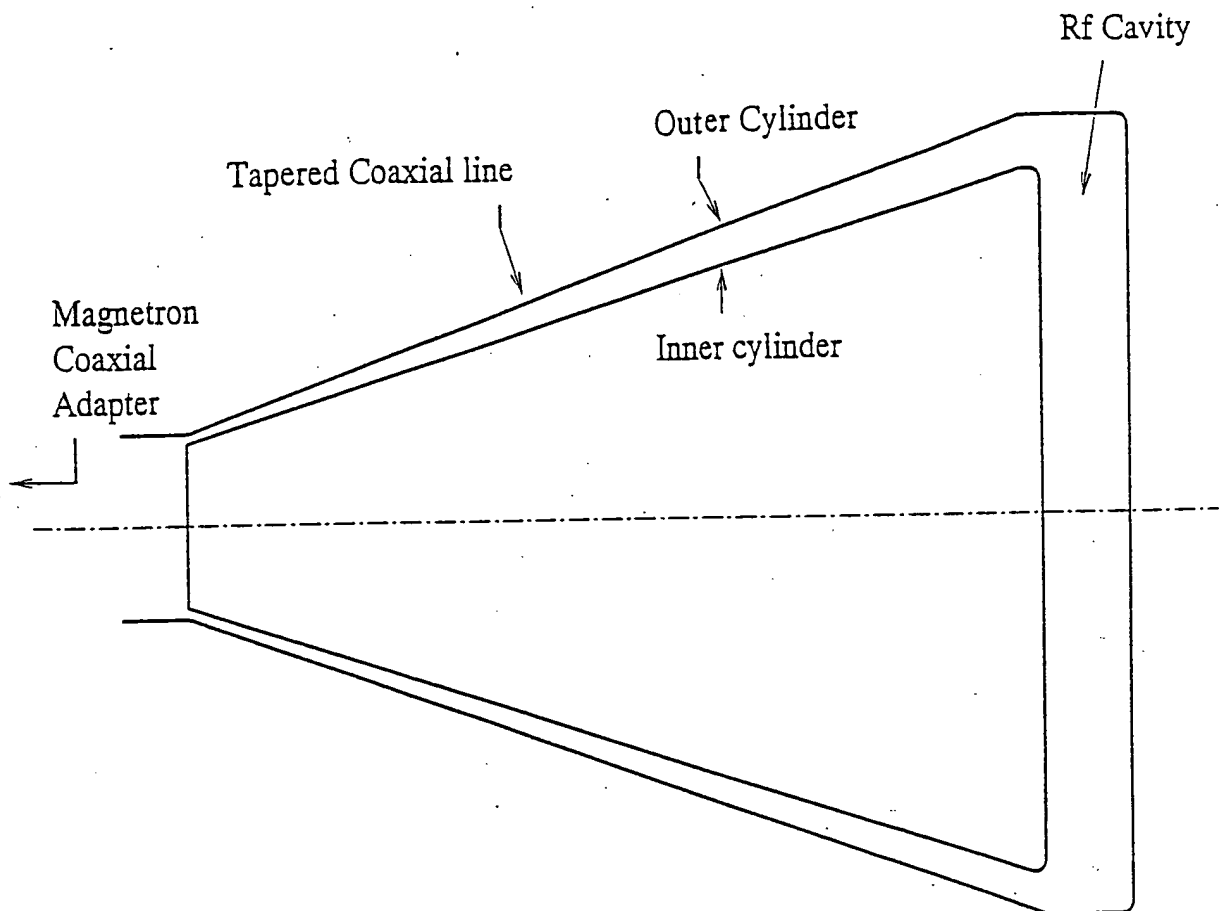


Figure 45: A magnetron feeding energy into the rf cavity. For simplicity a constant, low impedance, coaxial feed line is assumed. Voltage step-up occurs in the rf cavity.



RECEIVED

JUL 01 2004

TECH CENTER 2800

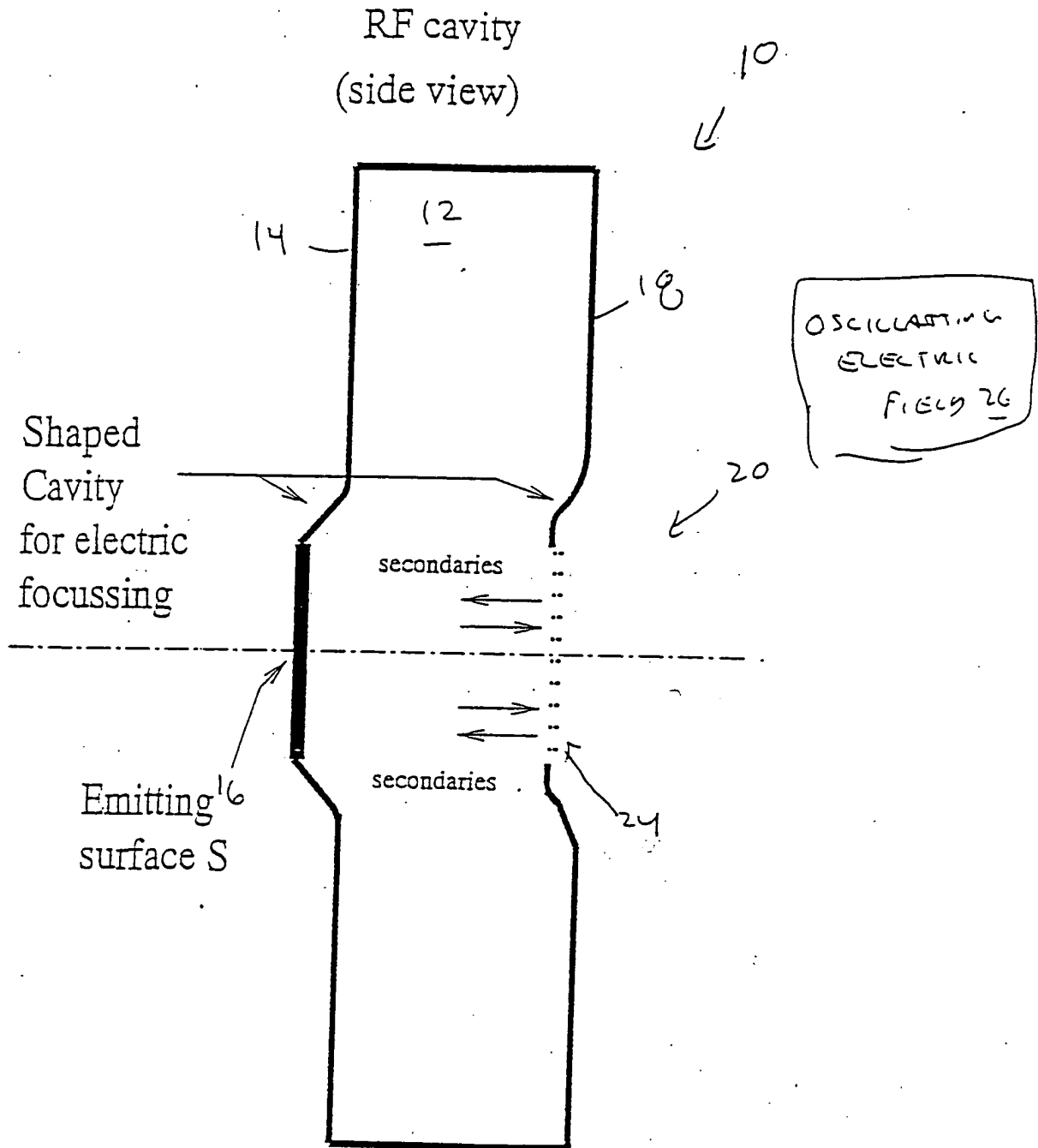


Figure 46: Schematic drawing of a possible design for electrostatic focusing in the MPG.